CANADIAN THESES ON MICROFICHE

I.S.B.N.

THESES CANADIENNES SUR MICROFICHE

National Library of Canada
Collections Development Branch

Canadian Theses on
Microfiche Service

Ottawa, Canada
K1A 0N4

Bibliothèque nationale du Canada
Direction du développement des collections

Service des thèses canadiennes
sur microfiche

NOTICE

The quality of this microfiche is heavily dependent upon the quality of the original thesis submitted for microfilming. Every effort has been made to ensure the highest quality of reproduction possible.

If pages are missing, contact the university which granted the degree.

Some pages may have indistinct print especially if the original pages were typed with a poor typewriter ribbon or if the university sent us a poor photocopy.

Previously copyrighted materials (journal articles, published tests, etc.) are not filmed.

Reproduction in full or in part of this film is governed by the Canadian Copyright Act, R.S.C. 1970, c. C-30. Please read the authorization forms which accompany this thesis.

AVIS

La qualité de cette microfiche dépend grandement de la qualité de la thèse soumise au microfilmage. Nous avons tout fait pour assurer une qualité supérieure de reproduction.

S'il manque des pages, veuillez communiquer avec l'université qui a conféré le grade.

La qualité d'impression de certaines pages peut laisser à désirer, surtout si les pages originales ont été dactylographiées à l'aide d'un ruban usé ou si l'université nous a fait parvenir une photocopie de mauvaise qualité.

Les documents qui font déjà l'objet d'un droit d'auteur (articles de revue, examens publiés, etc.) ne sont pas microfilmés.

La reproduction, même partielle, de ce microfilm est soumise à la Loi canadienne sur le droit d'auteur, SRC 1970, c. C-30. Veuillez prendre connaissance des formules d'autorisation qui accompagnent cette thèse.

THIS DISSERTATION
HAS BEEN MICROFILMED
EXACTLY AS RECEIVED

LA THÈSE A ÉTÉ
MICROFILMÉE TELLE QUE
NOUS L'AVONS REÇUE

NL-339 (r. 82/08)

Canada

Dynamical Stability of Crystals with and without Vacancies

by

Lebohang K. Moleko

Thesis submitted to the School of Graduate Studies
of the University of Ottawa in partial fulfilment
of the requirements for the degree
of Doctor of Philosophy in Physics

Physics Department
Science and Engineering Faculty
University of Ottawa
Ottawa, Canada
1984

UNIVERSITÉ D'OTTAWA
UNIVERSITY OF OTTAWA

TABLE OF CONTENTS

ABSTRACT

The dynamical stability of crystals with and without vacancies is investigated. The dynamics is treated with different approximations of the Self Consistent Phonon (SCP) theory. These are the Self Consistent Harmonic (SCH), the Self Consistent Einstein (SCE), SCH with cubic anharmonic shift (SCH + C) and the SCE with cubic anharmonic shift (SCEC) or (SCE + C). We apply these to study the stability of rare gas crystals (RGC's), Ne, Ar, Kr and Xe in a selective manner. The SCE, SCEC, SCE+C and SCEC+ vacancies approximations are also used to study the stability of a system of particles interacting via a pairwise repulsive Gaussian potential, referred to as the Gaussian core model (GCM). For crystals with vacancies only the SCEC was considered. The SCE and SCH gave instability temperatures T_I 10-300 times T_M depending on the system considered. Inclusion of the cubic term reduced T_I to 1.5-4 times T_M, also dependent on the systems. For defect free crystals the volume was set fixed at observed melting values in rare gas crystals (RGC's). The volume was determined from an Einstein approximation to the Improved Self Consistent (ISC) theory (the ISCE) for crystals with vacancies. The force constants are reduced when vacancies are created. The concentration of vacancies is determined by the dynamics in a consistent manner. The volumes of the RGC's predicted by the ISCE model are 1-2% lower than observed values depending on the pair potential. The predicted T_I's are 1.2-1.6 times T_M and the predicted instability densities ρ_I are 1.1-1.3 times observed ρ_I or melting densities ρ_M. Including vacancies induces crystal instability

not far above T_M, suggesting that a model of dynamics with vacancies may be largely responsible for the instability of real crystals. We find that the Lindemann rule holds for thermal melting with the ratio $\delta = 0.16$ with the more accurate approximations of the SCP theory. In the quantum limit the GCM was found to be unstable at very small Lindemann ratios $0.04 \leq \rho \leq 0.09$, thus suggesting that in this limit the Lindemann ratio takes a very wide range of values $0.04 \leq \delta \leq 0.35$, the higher values being for the Wigner solid and solid helium. In all cases the instability occurs suddenly with vibrational frequencies going discontinuously to imaginary unstable values.

ACKNOWLEDGEMENTS

I wish to extend firstly my most sincere and hearty gratitude to my supervisor Professor Henry R. Glyde who suggested the problem and provided dedicated and unwavering support throughout the course of this work. His unwaning interest and intricate physical insight helped in making an otherwise difficult and tedious problem very enjoyable. Partial financial support fron his NSERC grant was appreciated. The financial support from CIDA/WUSC is herewith acknowledged. The help and co-operation from CIDA/WUSC personnel was appreciated, in particular Gayle Turner, Andrew Hamilton, Eloise Burke and Stephen Wallace provided an easy atmosphere conducive to productivity at a difficult stage of my work. The study leave from N.U.L. is acknowledged.

The numerous interesting discussions with Dr. V. Sa-yakanit, the help I got on the use of the University computing facilities from Dr. M.G. Smoes, Mr. S. Hernadi and D.J. Singh were highly appreciated. The latter also made my stay in the workplace very habitable. To the many friends in the department whose sense of humour was responsible for my sanity in an otherwise dull environment I say thanks.

Secondly, I believe I should come back to home court and observe that charity begins at home, and in my case it is more appropriate. I wish to pay special tribute to people very deserving of it, my mom, my dad and my brother Tseliso who were collectively responsible for instilling in me the desire to pursue knowledge and also provided for it financially. The tolerance and love from all my brothers and sisters provided an environment suitable for nurturing an aspiring student. To you all 'Kea Leboha Bafokeng'.

Lastly but certainly not least my gratitude goes to three very special people, my wife Ithaopeng, my daughters Mpolokeng and Neo. I wish to say to you all, I would not have made it without your loving support. We made it together and to you I dedicate this work.

Finally I wish to thank Mrs. Lorraine Johnston who typed this manuscript.

CHAPTER 1

INTRODUCTION

In this thesis we investigate the instability of crystals through a model including mechanical vibrations and vacancies. We associate instability with vibrational mode frequencies becoming imaginary. We compare the instability temperatures T_I, instability densities ρ_I, with melting temperatures T_M and melting densities. In the past crystal instabilities have often been associated with melting of the crystals. Thus it is reasonable to review some literature on melting, in particular instability theories of melting as a background to this work. We emphasize that we do not treat crystal instability in the same breath as melting, we merely use melting parameters as a basis for comparison.

The theories of melting/freezing in three dimensions have a long and illustrious history, and can be divided into two broad categories. Firstly, are the theories often concentrating on only one of the phases, that associate a transition with the instability of the phase. These investigate the instability of either the solid phase or the fluid phase, analytically or by computer simulation. A few examples of these will be given at a later stage of this thesis. Secondly are the theories that study both phases and then identify a phase transition by equating the molar Gibb's free energies g_s and g_f of the solid and fluid at the same temperature and pressure.

i.e. $$g_f = g_s, \quad T_f = T_s, \quad P_f = P_s \qquad (1)$$

where T is the temperature and P the pressure. A few examples falling into this category are the Monte Carlo (MC) study of melting in a

Lennard-Jones system by Hansen and Verlet[1], in the one component plasma (Wigner solid) by Slattery and his co-workers[2] and by Pollock and Hansen[3], and analytically in sodium by Stroud and Ashcroft[4].

We highlight some examples falling into the first category, starting with fluid phase instability. Examples of the solid phase instability are left for a later consideration. Perhaps the most illustrious first principles theory of freezing is the pioneering work by Kirkwood and Monroe[5] (KM), who studied and derived an integral equation for the single particle distribution function $\rho(r)$. The integral equation when applied to Ar, gave periodic (crystalline) solutions as the temperature was lowered below a certain T_I. The KM work was followed much later by that of Brout[6]. His work was however unsatisfactory because the transition it predicted was continuous (second order). During the last decade, Raveché and his co-workers[7], studied the Yvon-Born Green hierarchy for the distribution function, finding crystalline solutions, in a region where the fluid phase was mechanically unstable. Recently, Ramakrishnan and Yussouff[8] derived an elegant theory based on the single particle distribution function $\rho(r)$, which is related to the direct correlation function (dcf) $C(q)$. They found a self consistent equation for $\rho(r)$ and expressed the free energy difference between the liquid and the solid in terms of $\rho(r)$. The dcf $C(q)$ is defined in terms of the static structure factor $S(q)$ as $S(q) = 1/(1 - C(q))$. This self consistent equation for $\rho(r)$ always has liquid like solutions. However for a critical value $C(q_1) = 0.85$ for a hexagonal lattice in two dimensions it also has a solid like solution. Here q_1 is the wave vector at the first peak of the static structure factor. This transition occurs discontinuously,

indicating a first order phase transition. For $C(q_1) \geq 0.85$, the free energy of the solid is found to be lower than that of the fluid, thus identifying the solid as the preferred equilibrium phase. A critical value for the dcf has been found for a Lennard-Jones system in 3 dimensions by Raveché and his co-workers[9]. In a similar Lennard-Jones system Hansen and Verlet found a critical static structure factor value $S(q_1) = 2.85 \pm 0.05$. This observation of a critical structure factor / dcf value led to a phenomenological rule "The Hansen-Verlet" freezing rule, stating that fluids freeze when $S(q_1)$ reaches the critical value of $S(q_1) = 2.85$. The observation on the relative magnitudes of the free energies of the liquid and solid suggests that the Hansen-Verlet rule (and perhaps the solid phase analogue the Lindemann rule[10]), express the structural dependence of the point at which the free energy of the solid and fluid are equal. Similarly, Jacobs[11] has developed a mean field theory of melting in which the difference in the free energy of the solid and liquid is evaluated. He finds that the difference vanishes at a constant value of δ; suggesting that the Lindemann rule is a rule on the free energy rather than on crystal stability. The Ramakrishnan-Youssouff ideas appear to be extendable to three dimensional systems.

We now focus our attention on the study of the instability of crystals. It has a long history going back to the beginning of the century with Lindemann's[10] pioneering work. He proposed that melting occurs when the root-mean square (rms) vibrational amplitude $\langle u^2 \rangle$ of the atoms about their equilibrium positions reaches a characteristic fraction $\delta = (\langle u^2 \rangle / R^2)^{\frac{1}{2}}$ of the interatomic spacing R. The Lindemann ratios δ have been determined just below T_M for a number of crystals

and found to be 0.16 ± 0.01[12-15]. This together with its freezing analogue allude to a geometric component to the transition which may be related to the stability of the solid and fluid phases. Perhaps here again, as in the case of the 2-D crystals discussed above, the free energy of the crystal just becomes too large relative to that of the fluid when the critical δ value is reached. In the computer simulation studies of Hoover and Ross[16], Raveché et al[7] and Stillinger and Weber[17], crystals were heated by up to 20% above T_M (or compressed by up to 10% below ρ_M) suggesting T_I lies significantly above T_M. Almost thirty years following Lindemann's pioneering work, Born[18] proposed that crystal instability (melting) was associated with the vanishing of the transverse elastic constants, since crystals support transverse modes at $\vec{q} = 0$ while fluids do not. In the last seventeen years some attention has been paid to the dynamical instability of solids against large vibrational amplitudes. The dynamics were treated within the self consistent phonon theory (SCP). This was sparked by the success of the SCP theory in predicting the accurate vibrational and thermodynamic properties of crystals with large amplitude vibrations[19-21]. It is this success that makes the SCP theory most suited for the study of crystal instabilities, since we are confident that both the vibrational and thermodynamic properties given by the theory, particularly when higher order anharmonic terms are included are accurate. The synopsis is given for different approximations to the SCP theory.

In an Einstein approximation to the self consistent harmonic approximation (SCH), Choquard[22] found no self consistent solutions above a certain critical temperature. The first order and second order SCP theory have been applied to the investigation of the stability of

the Wigner electron solid in 2 and 3 dimensions[19,20,23]. In the SCH approximation T_I was 20-40 times T_M predicted in MC calculations of Slatterly et al[2], Pollock et al[3] and the molecular dynamics (MD) of Hockney and Brown[20].

In a series of papers, Plakida, Siklos and their co-workers[24] investigated the instability of the SCP theory in several approximations in one and three dimensions. They found that inclusion of the leading term in second order reduced T_I substantially. Zubov[25] has included terms up sixth order in perturbation and found T_I of 1.3-1.5 times T_M for the rare gas crystals (RGC's). Matsubara and his co-workers[26] have applied the self consistent Einstein approximation (SCE) to study melting (instability) of metallic fine particles. This work has been succinctly reviewed by Hasegawa et al[27]. Their resulting T_I's are 20-50 times the observed T_M for the bulk material. The dependence of T_I on particle size is, however, as good as predicted by models based on free energy difference between solid and fluid phases. The high instability temperatures obtained in these models suggest that crystals melt for other reasons long before they are mechanically unstable. At absolute zero the one component plasma melts when sufficiently compressed. Here again the SCH predicts the crystal will remain stable to volumes much smaller than those suggested by MC calculations[28].

Melting in two dimensions has been a subject of great research effort in recent years, the most illustrious names coming to mind are Kosterlitz[29], Thouless[29], Halperin[30], Nelson[30] and Young[31]. Their ideas resulted in the KTHNY theory of melting based on the unbinding of dislocation pairs. Most of the theoretical, experimental and simulation studies of melting in 2-dimensions has been expertly discussed in three books[32]. In 2-dimensions melting is

believed to be due to an instability i.e. dislocation unbinding, whereas in 3-dimensions it is not; rather it is a first order phase transition.

It is known that as the crystal temperature rises the concentration of thermally created defects increases. Some work including vacancies in the dynamics has been done by Aksenov[33] and Adkhamov and his co-workers[34]. They find that inclusion of vacancies substantially reduced the instability temperatures. We also stress that this study is of collective effects and their influence on the instability of crystals. The instability does not originate locally around defects such as vacancies in this case. It is also conceivable that somebody might argue that the transition is solid-solid rather than solid-fluid, however we find that many modes become unstable just above the instability temperature, making it unlikely that the transformation is to another crystalline state or structure. Also in the Gaussian core model the instability densities of the fcc and bcc structures in the quantum limit are almost identical, thus suggesting that the transition at the instability is not to another crystalline state or structure.

Against this background we emphasize that here we are investigating crystal stability only, with less emphasis on attempting to relate it to melting. However we compare the instability temperatures (densities) with computer simulations T_I or (ρ_I) and melting parameters T_M (ρ_M), merely in an effort to measure our instability temperatures against others determined using similar approximations.

In this work the objective is twofold. Firstly we investigate the dependence of the instability temperatures T_I on the approximations made to the SCP theory, used to treat the dynamics in the systems we

study. Secondly we include vacancies in the Einstein approximation the SCP with cubic anharmonic term. The aim is to investigate whether atomic vibration and vacancy creation are the chief ingredients that eventually lead to the mechanical instability of crystals. We made an Einstein approximation to both the SCH and SCH + cubic anharmonic term. These are termed the self consistent Einstein (SCE) and the self consistent Einstein model with cubic term (SCEC or SCE + C), respectively. In the SCEC model the cubic term is iterated into the equations, while in the SCE + C the cubic term is merely added as a perturbation to the SCE. The model with vacancies is termed SCEC + V. These are the models used to investigate the stability of crystals here.

In the initial investigations of the instability of the RGC's with the SCH, SCE, SCEC, SCE + C and SCH + C models we set the crystal volume at the observed melting values for temperatures above T_M. Although this is rather arbitrary, it allows for direct comparisons between the different approximations. It would be difficult to make this comparison, had the volumes been determined from the models. This is because different models yield different values of the volumes. In the study of the SCEC + V model the volumes are determined from a companion approximation called the Improved Self Consistent Einstein Model (ISCE) with vacancies. It is essentially an Einstein approximation to the Improved Self Consistent theory (ISC)[35-37]. The ISC is presently the most accurate analytic model available for determining thermodynamic properties of crystals. We determine the temperature dependence of the isothermal bulk modulus and lattice dilation using different pair potentials from the ISCE + V model. This is done in order to test the reliability of the Einstein approximation made to

the ISC. Again we stress that the Einstein approximation is not meant to replace the more accurate ISC theory. We use it because of its appealing simplicity.

We find that T_I depends very sensitively on the approximation made to the SCP theory. The SCE and SCH T_I's are 10-300 times T_M. Higher order approximations, SCH + C, SCEC (SCE + C) give T_I 1.5-5 times T_M. The high T_I's found in SCE and SCH are an artifact of the approximations rather than the SCP theory itself. The SCEC + V gives T_I about 1.2-1.6 times T_M. This is in part due to the fact that the ISCE predicts volumes smaller than the observed. The lattice dilations and isothermal bulk moduli from the ISCE also depend sensitively on the interatomic potential. At T_I the phonon mode frequencies go discontinuously from finite stable values to imaginary unstable values, characteristic of a first order transition.

In chapter 2 we review the SCP theory, starting with the SCH approximation and its reduction to the SCE model. The higher order approximations, the SCH + C and the SCEC/SCE + C models are also presented in this chapter. The corresponding Helmholtz free energies are also given here. In chapter 3 we derive the equations for the dynamics of a system containing vacancies. We test the ISCE + V in chapter 4. In chapter 5 we investigate the stability of the RGC's with the models outlined in chapters 2 and 3. We also investigate the stability of the Lennard-Jones system and we compare our results with the MC simulations of Hoover and Ross[15] and Raveché and his co-workers[9]. The stability of the Gaussian core model in the Einstein approximation to the SCP theory is investigated, and the results are compared with the MD simulations of Stillinger and Weber[17]. Our investigation is done in the classical as well as quantum limit not accessible with the MD technique. In chapter 6 we discuss our results and draw conclusions from our study.

REFERENCES

(1) J.P. Hansen and L. Verlet, Phys. Rev. 184, 151 (1969).

(2) W.L. Slatterly, G.D. Doolen and H.E. DeWitt, Phys. Rev. A26, 2255 (1982), A21, 2087 (1980).

(3) E.L. Pollock and J.P. Hansen, Phys. Rev. A8, 310 (1973).

(4) D. Stroud and N.W. Ashcroft, Phys. Rev. B5, 371 (1972).

(5) J.G. Kirkwood and E. Monroe, J. Chem. Phys. 8, 845 (1940); J.G. Kirkwood in Phase Transformations in Solids, ed. by R. Smoluchowski, J.E. Mayer and W.A. Neyl (Wiley, New York, 1951).

(6) R. Brout, Physica, 29, 1041 (1963); Phase Transitions, (Benjamin, New York) (1964).

(7) R.F. Kayser, Jr. and H.J. Raveché, Phys. Rev. B22, 424 (1980); H.J. Raveché and R.F. Kayser, Jr., J. Chem. Phys. 68, 3633 (1978); H.J. Raveché and C.A. Stuart, J. Chem. Phys. 65, 2305 (1976); J. Math. Phys. 17, 1949 (1976), J. Chem: Phys. 63, 1099 (1975).

(8) T.V. Ramakrishnan, Phys. Rev. Lett. 48, 541 (1982); T.V. Ramakrishnan and M. Yussouff, Phys. Rev. B19, 2775 (1979), Solid State Comm. 21, 389 (1977).

(9) W.B. Street, H.J. Raveché and R.D. Mountain, J. Chem. Phys. 61, 1960 and 1970 (1974).

(10) F.A. Lindemann, Phys. Z 11, 609 (1911)

(11) R.L. Jacobs, J. Phys. C 16, 273 (1983).

(12) V.V. Goldman, J. Phys. Chem. Solids 30, 1090 (1969).

(13) J.P. Hansen, Phys. Rev. A2, 221 (1970).

(14) E.L. Pollock and J.P. Hansen, Phys. Rev. A8, 310 (1973).

(15) H.R. Glyde and R. Taylor, Phys. Rev. B5, 1206 (1972).

(16) W.G. Hoover and M. Ross, Contemp. Phys. 12, 339 (1971) and references therein.

(17) F.H. Stillinger and T.A. Weber, Phys. Rev. B22, 3790 (1980) and references therein.

(18) M. Born, J. Chem. Phys. 7, 591 (1939).

(19) H.R. Glyde and G.H. Keech, Ann. Phys. (New York), 127, 330 (1980).

(20) R.C. Albers and J.E. Gubernatis, Phys. Rev. B23, 2783 (1981).

(21) R.W. Hockney and T.R. Brown, J. Phys. C 8, 1812 (1975).

(22) P. Choquard, The Anharmonic Crystal (Benjamin, New York) (1967).

(23) A.A. Kugler, Ann. Phys. (New York), 53, 133 (1969); H. Fukuyama and P.M. Platzmann, Solid State Comm. 15, 617 (1974); P.M. Platzmann and H. Fukuyama, Phys. Rev. B10, 3180 (1974).

(24) N.M. Plakida and T. Siklós, Acta Phys. Acad. Sci. Hung. 45, 37 (1978) and references therein.

(25) V.I. Zubov, Phys. Stat. Sol. (b) 88, 43 (1978); 87, 385 (1978).

(26) T. Matsubara, Y. Iwase and A. Momokita, Prog. Theor. Phys. Japan 58, 1102 (1977).

(27) M. Hasegawa, K. Hashimo and M. Watabe, J. Phys. F10, 619 (1980).

(28) D. Ceperly, Phys. Rev. B18, 3126 (1978).

(29) J.M. Kosterlitz and D.J. Thouless, J. Phys. C6, 1181 (1973), J.M. Kosterlitz ibid 7, 1046 (1974).

(30) B.I. Halperin and D.R. Nelson, Phys. Rev. Lett. 41, 121 (1975); D.R. Nelson and B.I. Halperin, Phys. Rev. B19, 2457 (1979).

(31) A.P. Young, Phys. Rev. B19, 1855 (1979).

(32) Ordering in two dimensions, ed. by S.K. Sinha (North Holland Amsterdam, 1980), Proceedings of the Ninth Midwest Solid State Theory Symposium "Melting, Localization and Chaos" ed. by R.K. Kalia and P. Vashishta (North Holland Amsterdam, 1981). Nonlinear Phenomena at Phase Transitions and Instabilities ed. by T. Riste (Plenum 1981).

(33) V.L. Aksenov, Sov. Phys. Solid State 14, 1718 (1973).

(34) A.A. Adkhamov, V.A. Gumovskii and V.I. Lebedev, Sov. Phys. Doklady 25, 928 and 932 (1931); Rev. Int. Hautes Temper. Retract. (France) 17, 59 (1980).

(35) H.R. Glyde and M.L. Klein, Crit. Rev. Solid State Sci. 2, 181 (1971).

(36) V.V. Goldman, G.K. Horton and M.L. Klein, J. Low Temp. Phys. 1, 391 (1969).

(37) M.L. Klein and T.R. Koehler in Rare Gas Solids ed. by M.L. Klein and J.A. Venables Vol. I (Academic Press, New York 1976).

CHAPTER 2

CHAPTER 2

2.1 INTRODUCTION

In this chapter we give a brief outline of the self consistent phonon theory. In real cyrstals at all temperatures, the atoms are in a state of continual motion. In the Born-Oppenheimer approximation it is assumed that the potential energy of the crystal, where the displacements of the atoms from their equilibrium positions are small, can be written as a power series involving the displacements $u_\alpha(\ell)$ of the nuclei.

$$V = V_o + V_1 + V_2 + \ldots \tag{2.1}$$

where

$$V_1 = \sum_{\alpha\ell} \frac{\partial V}{\partial r_\alpha(\ell)} u_\alpha(\ell)$$

$$V_2 = \sum_{\substack{\alpha\beta \\ \ell\ell'}} \frac{\partial^2 V}{\partial r_\alpha(\ell)\, \partial r_\beta(\ell')} u_\alpha(\ell)\, u_\beta(\ell') \tag{2.2}$$

The derivatives are evaluated at the equilibrium positions of the atoms. In the harmonic approximation the series, equation (2.1) is truncated at V_2, and since the crystal is in equilibrium $V_1 = 0$. Then the resulting quadratic Hamiltonian is solved for normal vibrational modes[1],[2]. A crystal in which the forces are strictly harmonic, has no coefficient of expansion, the elastic constants are independent of temperature and $C_v = C_p$, all of these properties are not possessed by real crystals. However, if the derivatives are evaluated at the mean positions which the atoms actually occupy at a temperature T, the force constants are then temperature dependent. This is called the quasi-harmonic approximation. The vibrational mode frequencies or phonons describing

travelling waves through the crystal are obtained as the roots of the dynamical matrix D from the eigenvalue equation

$$\omega^2_{q\lambda} = \sum_{\alpha,\beta} \vec{\varepsilon}_\alpha (q\lambda) \overleftrightarrow{D}_{\alpha\beta} (q) \vec{\varepsilon}_\beta (q\lambda) \qquad \ldots \qquad (2.3)$$

where the polarization vectors $\vec{\varepsilon}_\alpha(q\lambda)$, and $\vec{\varepsilon}_\beta(q\lambda)$ satisfy the following orthogonality and closure relations

$$\vec{\varepsilon}_\alpha(q\lambda) \cdot \vec{\varepsilon}_\alpha(q\lambda') = \delta_{\lambda\lambda'}$$

$$\sum_\lambda \vec{\varepsilon}_\alpha(q\lambda) \vec{\varepsilon}_\beta(q\lambda) = \delta_{\alpha\beta} \qquad \ldots \qquad (2.4)$$

The dynamical matrix is given by

$$D_{\alpha\beta}(\vec{q}) = \frac{1}{M} \sum_\ell{}' (e^{-i\vec{q}.\vec{R}_\ell} - 1) \phi_{\alpha\beta}(0\ell) \qquad \ldots \qquad (2.5)$$

$\phi_{\alpha\beta}(0\ell)$ are the force constants. The force constants describe the change in the crystal potential due to the displacements $u_\alpha(0)$ and $u_\beta(\ell)$ of an ion when all its neighbours are held fixed at their equilibrium positions. In the harmonic and quasi-harmonic approximations the force constants are given by

$$\phi_{\alpha\beta}(0\ell) = \nabla_\alpha(0) \nabla_\beta(\ell) V(r_{0\ell}) \qquad \ldots \qquad (2.6)$$

where

$$\nabla_\alpha = \frac{\partial}{\partial r_\alpha}$$

and $V(r_{0\ell})$ is the interatomic potential assumed here to be pair-wise and only dependent on the magnitude of the atomic separation. If the crystal is only weakly anharmonic, the cubic and quartic terms in (2.1) are retained[3]. These terms are regarded to be small and are handled

by perturbation theory. The quartic term contributes in first order while the cubic term contributes in second order. The perturbation approach however fails for anharmonic crystals such a helium[4] whose atoms execute large vibrational amplitude motion. Even for classical crystals like Kr, this approach breaks down at temperatures about 40% of the melting temperature[5]. The procedure that has been found to be successful is the one that regards the motion of all the atoms to be affected by that of its neighbours. This is the self consistent approach here called the Self Consistent Phonon theory. In section 2.2 we discuss the general features of the self consistent phonon (SCP) theory. In (2.3) we present the first order approximation to the SCP theory called the Self Consistent Harmonic Approximation (SCH), and in (2.4) we reduce the SCH to the Einstein model (SCE). In section (2.5) we discuss the higher order SCP theory, and in (2.6) we reduce the SCH + C to the corresponding Einstein form SCEC/ISCE. The last section (2.7) discusses the Helmholtz free energies both in first and second order SCP theory.

2.2 SELF CONSISTENT PHONON THEORY

The basis of this theory is an observation that the motion of an atom in a crystal, when its vibrational amplitudes are large should not be treated in an approximation where the surrounding equivalent atoms are fixed at their lattice sites. Rather the motion of all atoms should be incorporated in a self consistent manner.

2.3 SELF CONSISTENT HARMONIC APPROXIMATION (SCH)

The lowest-order full SCP theory is the SCH approximation. The theory is most easily derived variationally through free energy minimization. The derivations due to Boccara and Sarma[6], Gillis, Werthamer and Koehler[7] are the tenet of the development of the SCH theory from a variational principle. The theory has also been derived by a number of other different techniques[8-13]. In this approximation all the even-order terms (2.1) are retained. The frequency of a phonon having a wave vector $\vec{q}$ and a branch λ is given by the same equation as in (2.3), but the force constants $\phi_{\alpha\beta}(0\ell)$ in equation (2.5), are thermodynamically averaged over the vibrational distributions of the atoms. The force constants are given by

$$\phi_{\alpha\gamma}(0\ell) = \langle \nabla_\alpha(0)\ \nabla_\gamma(\ell)\ V(\vec{r}_{0\ell}) \rangle$$

$$= [(2\pi)^3 |\vec{\Lambda}|]^{-\frac{1}{2}} \int d\vec{u}\ \exp(-\tfrac{1}{2}\ \vec{u}.\vec{\Lambda}.\vec{u})$$

$$\times\ \vec{\nabla}_\alpha(0)\ \vec{\nabla}_\gamma(\ell)\ V(\vec{r}_{0\ell}) \qquad \ldots \qquad (2.7)$$

where the vibrational distribution is assumed to be Gaussian with width

$$\Lambda_{\alpha\gamma}(0\ell) = \langle u_\alpha(0\ell)\ u_\gamma(0\ell) \rangle$$

$$= \frac{\hbar}{MN} \sum_{q\lambda} (1 - e^{-i\vec{q}.\vec{R}_\ell})\ \varepsilon_\alpha(q\lambda)\ \varepsilon_\gamma(q\lambda)$$

$$\times\ \coth(\beta\hbar\omega_{q\lambda}/2)/\omega_{q\lambda} \qquad \ldots \qquad (2.8)$$

where h, M, N, λ have their usual meaning α, γ being x, y or z and $\beta = 1/K_\beta T$. The self consistency equations for the SCH approximation are (2.3), (2.7) and (2.8).

2.4 SELF CONSISTENT EINSTEIN APPROXIMATION (SCE)

The SCE approximation is obtained from the SCH approximation by neglecting all correlations among particle displacements in equation (2.8). The square of the SCE frequency is defined as the average of the square of the SCH frequency. Thus

$$\omega_E^2 = \frac{1}{3N} \sum_{q\lambda} \omega_{q\lambda}^2 \qquad \ldots \qquad (2.9)$$

$$= \frac{1}{3N} \sum_{q\lambda} \sum_{\alpha\beta} \vec{\varepsilon}_\alpha(q\lambda) \overleftrightarrow{D}_{\alpha\beta}(q) \vec{\varepsilon}_\beta(q\lambda)$$

$$= \frac{1}{3N} \sum_{q,\lambda} \sum_{\alpha\beta} \vec{\varepsilon}_\alpha(q\lambda) \frac{1}{M} \sum_{\ell}{}' (e^{-i\vec{q}.\vec{R}_\ell} - 1)\, \phi_{\alpha\beta}(0\ell)\, \vec{\varepsilon}_\beta(q\lambda)$$

$$= \frac{1}{3M} \sum_{\alpha,\ell}{}' \phi_{\alpha\alpha}(0\ell) \qquad \ldots \qquad (2.10)$$

where we have used the following properties to get (2.10)

$$\sum_{\lambda} \vec{\varepsilon}_\alpha(q\lambda)\, \vec{\varepsilon}_\beta(q\lambda) = \delta_{\alpha\beta}$$

$$\sum_{q} e^{-i\vec{q}.\vec{R}(0\ell)} = N\delta_{0\ell} \qquad \ldots \qquad (2.11)$$

The SCE force constant is given by

$$\phi_{\alpha\alpha}(0\ell) = \left\langle \frac{d^2V(r_{0\ell})}{dr^2} + \frac{2}{r}\frac{dV}{dr} \right\rangle \quad \ldots \quad (2.12)$$

$$= \left(\frac{1}{2\pi\Lambda}\right)^{3/2} \int d\vec{u}\, e^{-u^2/2\Lambda} \left[\frac{d^2V}{dr^2} + \frac{2}{r}\frac{dV}{dr}\right] \quad \ldots \quad (2.13)$$

In equation (2.13) we have made an Einstein approximation to $\vec{\Lambda}_{\alpha\beta}(0\ell)$ in equation (2.8), by replacing all frequencies by the average frequency ω_E. Thus

$$\langle u_\alpha(0\ell)\, u_\beta(0\ell)\rangle_E = 2\langle u^2{}_\alpha(0)\rangle \delta_{\alpha\beta}$$

$$= \frac{\hbar}{M\omega_E} \coth(\beta\hbar\omega_E/2) = \Lambda \quad \ldots \quad (2.14)$$

Hence equation (2.10) reduces to

$$\omega^2{}_E = \frac{1}{3M} \sum_{\tau}{}' \left(\frac{1}{2\pi\Lambda}\right)^{3/2} \int d\vec{u}\, e^{-u^2/2\Lambda} \left(\frac{d^2V}{dr^2} + \frac{2}{r}\frac{dV}{dr}\right) \quad \ldots \quad (2.15)$$

where $\vec{r} = \vec{\tau} + \vec{u}$, $\vec{\tau}$ being the lattice vector associated with the ℓ^{th} atom. In the SCE approximation the Lindemann ratio is given by

$$\delta^2 = \langle u^2\rangle / R^2$$

$$= 3\langle u_\alpha^2\rangle / R^2 \quad \ldots \quad (2.16)$$

The basic self consistency equations for the SCE model are equations (2.14) and (2.15); they are solved iteratively at a given temperature and a corresponding lattice parameter. The SCE model can also be derived variationally from the free energy. This variational derivation will be done in the next chapter for crystals containing vacancies. We note here that we recover equation (2.15) from equation (3.21) of the following chapter if the vacancy concentration is zero.

2.5 HIGHER ORDER SCP THEORY

The leading new term beyond the SCH approximation is the cubic anharmonic term representing a three phonon process to second order.. This is usually added as a perturbation to the first order self consistent phonon frequencies. When the cubic anharmonic term is included, the dynamical independence of the different vibrational modes is destroyed thus leading to phonons with finite lifetimes. In this approximation, the phonon frequency is usually identified with the frequency at which the response of the crystal to an external perturbation of wavevector $\vec{q}$ and polarization vector $\vec{\epsilon}_\alpha(q\lambda)$ is a maximum. This response function is

$$A(\vec{q}\lambda;\omega) = \frac{8\omega^2_{q\gamma}\,\Gamma(q\lambda;\omega)}{[-\omega^2 + \omega^2_{q\lambda} + 2\omega_{q\lambda}\,\Delta(q\lambda;\omega)]^2 + [2\omega_{q\lambda}\,\Gamma(q\lambda;\omega)]^2} \quad \ldots \quad (2.17)$$

where $\Delta(q\lambda;\omega)$ is the shift in the phonon frequency and $\Gamma(q\lambda;\omega)$ is the inverse of the phonon lifetime due to the addition of the cubic anharmonic term.

$$\Delta(q\lambda;\omega) = -(2\hbar^2)^{-1} \sum_{1,2} |\langle V(q\lambda;\,1,2)\rangle|^2\, M(1,2;\omega) \quad \ldots \quad (2.18)$$

$$\Gamma(q\lambda;\omega) = -(2\hbar^2)^{-1} \sum_{1,2} |\langle V(q\lambda;1,2)\rangle|^2\, J(1,2;\omega) \quad \ldots \quad (2.19)$$

where $\langle V(q\lambda;1,2)\rangle$ is the Fourier transform of the cubic force constant. $M(1,2;\omega)$ and $J(1,2;\omega)$ are given by Glyde[14]

$$M(1,2;\omega) = (n_1 + n_2 + 1)\left[\frac{1}{\omega + \omega_1 + \omega_2} - \frac{1}{\omega - (\omega_1 + \omega_2)}\right] - (n_2 - n_1)x$$

$$\left[\frac{1}{\omega + \omega_2 - \omega_1} - \frac{1}{\omega - \omega_2 + \omega_1}\right] \quad \ldots \quad (2.20)$$

$$J(1,2;\omega) = -\{(n_1 + n_2 + 1)\pi[\delta(\omega + \omega_1 + \omega_2) - \delta(\omega - (\omega_1 + \omega_2))]$$

$$-(n_2 - n_1)\,\pi[\delta(\omega + \omega_2 - \omega_1) - \delta(\omega - \omega_2 + \omega_1)]\} \quad \ldots \quad (2.21)$$

$$\omega_1 = \omega_{q_1\lambda_1} \quad \text{and} \quad n_1 = n(\omega_1) = (e^{\beta\hbar\omega_1} - 1)^{-1}.$$

If $\Delta(q\lambda;\omega)$ and $\Gamma(q\lambda;\omega)$ are not strongly dependent on ω, the response function is a Lorentzian function, and the phonon frequency is given by the zero of the first term in the denominator of the response function (2.17) i.e. by

$$\omega^2 = \omega^2_{q\lambda} + 2\omega_{q\lambda}\,\Delta(q\lambda;\omega) \quad \ldots \quad (2.22)$$

Since $\Delta(q\lambda;\omega)$ is negative and becomes more so as the temperature increases, it is to be expected that at a high enough temperature, ω^2 in equation (2.22) becomes negative, thus giving imaginary frequencies. In this model denoted SCH + cubic (SCH + C) the instability of the crystal is associated with the position of the peak in (2.17) for a specific phonon going to zero (or below zero) thus signalling an "overdamped" mode.

2.6 HIGHER ORDER SCP THEORY IN THE EINSTEIN APPROXIMATION

The full SCH + C model involves a lengthy calculation since the SCH calculation is itself lengthy and $\Delta(q\lambda;\omega)$ is also a lengthy expression and we must search many frequencies at each temperature to determine which one becomes unstable first. We therefore seek an Einstein approximation to (2.22). As in the SCE we define the Einstein frequency including the cubic term as the average over all q and λ of (2.22),

$$\omega^2(\text{SCE} + \text{C}) \quad \frac{1}{3N} \sum_{q,\lambda} [\omega^2_{q\lambda} + 2\omega_{q\lambda}\, \Delta(q,\lambda;\omega)] \qquad \ldots \qquad (2.23)$$

The first term in equation (2.23) is just the SCE frequency given in section 2.4. In the second term on the right hand side of equation (2.23), if we approximate all the frequencies by ω_E equation (2.23) reduces to (see Appendix for details)

$$\omega^2(\text{SCE} + \text{C}) = \omega^2_E + 2\omega_E\, \bar{\Delta}(\omega_E) \qquad \ldots \qquad (2.24)$$

where

$$\bar{\Delta}(\omega_E) = -\frac{2.36\hbar}{12M^3\omega_E^4} \cdot [2n(\omega_E) + 1] \times \sum_{\ell} \left(\left\langle \frac{d^3}{dr^3} V(R_\ell + u) \right\rangle_E\right)^2 \qquad \ldots \qquad (2.25)$$

Equation (2.25) follows directly from (2.23) by replacing all $\omega_{q\lambda}$ with ω_E and retaining the leading term of the cubic coefficient, except for the factor of 2.36. While it is expected that $\bar{\Delta}(\omega_E)$ will have the correct dependence on mass, temperature, and crystal potential, it will almost certainly be too small. This is because we have replaced all the frequencies $\omega_{q\lambda}$; some of which are very small transverse frequencies by a large ω_E which is approximately 75% of the maximum frequency in the Brillouin zone; and $\bar{\Delta}(\omega_E)$ is inversely proportional to ω_E^4. We therefore chose ths single factor of 2.36 so that the Einstein frequency given by (2.24) became unstable at the same temperature for argon as the least stable phonons in the full SCH + C. The same factor was used for all the systems studied. In the instability study using equation (2.24) two models are considered. In the first one termed the Self Consistent Einstein model + cubic term (SCE + C), we iterated equations (2.14) and (2.15) to get ω_E and the shift $\bar{\Delta}(\omega_E)$ is added as a perturbation in equation (2.24). In the second model denoted self consistent Einstein

model with cubic term iterated (SCEC), we iterated equations (2.15), (2.24), (2.25) and (2.14) with the frequency ω(SCEC) replacing ω_E is equation (2.15) to calculate the Gaussian width Λ used in equation (2.14) and (2.25). The SCEC generally gave lower instability temperatures than the SCE + C model by about 2-3%. The models outlined in this chapter were used selectively to investigate the stability of rare gas solids Ne, Ar, Kr and Xe. The SCEC will also be applied to investigate the stability of crystals with vacancies, this will be developed in chapter 3. The SCEC will also be applied to investigate the stability of the Gaussian core model (GCM).

2.7 FREE ENERGIES

The Helmholtz free energy in the SCH approximation is

$$F_{SCI} = \frac{1}{2} \sum_{i \neq j} \langle V(r_{ij}) \rangle + \frac{1}{2} \sum_{q\lambda} \hbar\omega_{q\lambda} [2n(\omega_{q\lambda}) + 1)] + K_\beta T \sum_{q\lambda} \ln [2 \sinh (\tfrac{1}{2} \hbar \omega_{q\lambda} / K_\beta T)] \quad \ldots \quad (2.26)$$

In the SCH + C, the corresponding free energy is[15]

$$F_{SC2} = F_{SC1} + \Delta F_3 \quad \ldots \quad (2.27)$$

$$\Delta F_3 = - \frac{1}{3!\hbar} \sum_{1,2,3} |\langle V_3(1,2,3) \rangle|^2 \, W(1,w,3) \quad \ldots \quad (2.28)$$

$$W(1,2,3) = \frac{(n_1 + 1)(n_2 + n_3 + 1) + n_2 n_3}{\omega_1 + \omega_2 + \omega_3} + 3 \frac{n_1(n_2 + n_3 + 1) - n_2 n_3}{\omega_1 + \omega_3 - \omega_1} \quad (2.29)$$

Here $1 = q_1\lambda_1$ and $n_1 = n(\omega_{q_1\lambda_1})$.

In the Einstein approximation the Helmholtz free energy reduces to

$$F = F_{SCE} + \Delta F \qquad \ldots \qquad (2.30)$$

where

$$F_{SCE} = \frac{1}{2} \sum_{i \neq j} \langle V(r_{ij}) \rangle + 3N K_\beta T \ln(2\sinh(\beta\hbar\omega_E/2))$$

$$- \frac{3}{4} N \hbar \omega_E \coth(\beta\hbar\omega_E/2) \qquad \ldots \qquad (2.31)$$

and

$$\Delta F = \frac{-2.36\hbar^2(12n^2(\omega_E) + 12n(\omega_E) + 1)}{144\ \omega_E^4\ M^3}$$

$$x \sum_{\ell} \left(\langle \frac{d^3V}{dr^3} (R_\ell + u) \rangle_E\right)^2 \qquad \ldots \qquad (2.32)$$

To get (2.31) and (2.32) we have replaced $\omega_{q\lambda}$ by a single ω_E and $n(\omega_{q\lambda})$ by $n(\omega_E)$. The factor 2.36 is the same as in previous section. The improved self consistent free energy (2.30) will be used to determine some bulk thermodynamic properties of rare gas crystals in chapter 4.

REFERENCES

(1) A.A. Maradudin, E.W. Montioll, G.H. Weiss and G.H. Ipatova, Solid State Physics, ed. by F. Seitz and D. Turnbull. Supplement 3 (1971); Theory of Lattice Dynamics in the Harmonic Approximation (Academic Press New York and London 1971).

(2) A.A. Maradudin in Dynamical Properties of Solids, ed. by G.K. Horton and A.A. Maradudin, volume 1. Crystalline Solids Fundamentals (North Holland 1974).

(3) R.A. Cowley. Adv. Phys. 12, 421 (1963), Rep. Prog. Phys. 31, 123 (1968).

(4) F.W. De Wette, L.H. Nosanow and N.R. Werthamer. Phys. Rev. 162, 824 (1967).

(5) M.L. Klein and G.K. Horton. Proc. 11th Conf. Low Temp. Phys. St. Andrews, Scotland (1968).

(6) N. Boccara and G. Sarma. Physics 1, 219 (1965).

(7) N.S. Gillis, N.R. Werthamer and T.R. Koehler. Phys. Rev. 165, 951 (1968).

(8) T.R. Koehler. Phys. Rev. Lett. 17, 89 (1966).

(9) H. Horner. Z. Phys. 205, 72 (1967).

(10) H.R. Glyde. Can. J. Phys. 49, 761 (1971).

(11) V. Sa-yakanit and H.R. Glyde. J. Phys. C6, 1166 (1973).

(12) P. Choquard. The anharmonic crystal (W.A. Benjamin, New York 1967).

(13) N.M. Plakida and T. Siklos. Phys. Stat. Sol. 33, 103, 113 (1969).

(14) H.R. Glyde. Can. J. Phys. 52, 2281 (1974).

(15) H.R. Glyde and M.L. Klein. Crit. Rev. Solid State Sci. 2, 181 (1971).

CHAPTER 3

6 Crystals Containing Vacancies

3.1 Introduction

3.2 Model

3.3 Dynamics

3.4 Concentration of Vacancies

3.5 Einstein Approximation for Crystals with Vacancies (SCEC + V) and (ISCE + V)

CHAPTER 3

3.1 INTRODUCTION

The correct description of many bulk thermodynamic properties of real crystals can be effected by considering the anharmonicity of lattice phonons. At sufficiently high temperatures, there is also a large concentration of thermal defects. In particular at the triple points of rare gas crystals large concentrations of vacancies have been observed. For instance the following concentrations have been observed, in Ne[1] $C_T = 3 \times 10^{-4}$, in Ar[2] $C_T \leq 2 \times 10^{-4}$ while in Kr[3] $C_T = 3.2 \times 10^{-3}$ at their triple points, in xe[4] vacancy concentration of 8.2×10^{-3} has been observed at the triple point. The theoretical calculation of Glyde[5] and Glyde and Venables[6] in Kr found concentrations approximately one tenth of the experimental observation of Losee and Simmons[3]. Squire and Hoover[7] in their Monte Carlo calculation also find concentrations approximately one tenth the Losee and Simmons values for Kr. The high concentration of vacancies should affect the dynamics of the crystals particularly at high temperatures. In particular we expect that vacancies play an important role in the stability of crystals. In this chapter we derive the equations describing crystals with vacancies within the SCP theory in first order. In second order the equations can easily be derived.

3.2 MODEL

We consider a crystal of N identical atoms of Mass M on a Bravais lattice with N_L sites. The crystal has $n = N_L - N$ vacant sites.

N is fixed while N_L and n can vary with temperature. We assume that the atoms interact via a pairwise potential. The Hamiltonian of this system is

$$H = \sum_{\ell=1}^{N_L} T_\ell \sigma_\ell + \frac{1}{2} \sum_{\ell\ell'}^{N_L} V(r_{\ell\ell'}) \sigma_\ell \sigma_{\ell'} \qquad \ldots \qquad (3.1)$$

where $T_\ell = P_\ell^2/2M$ is the kinetic energy of the atom ℓ and $V(r_{\ell\ell'})$ the interatomic pair potential. The parameter σ_ℓ indicates the occupancy of site ℓ.

$$\sigma_\ell = \begin{cases} 1 & \text{if the site } \ell \text{ is occupied} \\ 0 & \text{if the site } \ell \text{ is vacant} \end{cases} \qquad \ldots \qquad (3.2)$$

This approach is similar to Stripp and Kirkwood's[8] work. We transform to new occupation parameters $C_\ell = 1 - \sigma_\ell$, defined

$$C_\ell = \begin{cases} 0 & \text{if site } \ell \text{ is occupied} \\ 1 & \text{if site } \ell \text{ is vacant} \end{cases} \qquad \ldots \qquad (3.3)$$

where clearly

$$\sigma_\ell + C_\ell = 1 \qquad \ldots \qquad (3.4)$$

$$\sum_{\ell}^{N_L} C_\ell = n \qquad \ldots \qquad (3.5)$$

$$C = \langle C_\ell \rangle = \frac{1}{N_L} \sum_{\ell}^{N_L} C_\ell = \frac{n}{N_L} = \frac{n}{n+N} \qquad \ldots \qquad (3.6)$$

and $\langle C_\ell \rangle$ is the average concentration of vacancies. In terms of the complementary variables the crystal Hamiltonian is

$$H = \sum_{\ell}^{N_L} T_\ell (1 - C_\ell) + \frac{1}{2} \sum_{\ell\ell'}^{N_L} V(r_{\ell\ell'})(1 - C_\ell)(1 - C_{\ell'}) \qquad \ldots \qquad (3.7)$$

We wish to approximate the ground state and the low lying excited states of our system by a simple model system in which the calculations can be easily performed. The simplest choice is the one in which the interactions are harmonic whose Hamiltonian is

$$H_o = \sum_{\ell}^{N} T_\ell + \frac{1}{2} \sum_{\ell\ell'}^{N} V_H(r_{\ell\ell'}) \qquad \ldots \quad (3.8)$$

where

$$V_H = V(R_{\ell\ell'}) + \frac{1}{2} \vec{u}(\ell,\ell') \cdot \overleftrightarrow{\phi}_{\alpha\beta}(\ell,\ell') \vec{u}(\ell,\ell') \qquad \ldots \quad (3.9)$$

We assume that our model system also has n vacancies, but that their presence does not change or affect the energy or the interactions between the atoms. In the hypothetical system the phonon states and the vacancy positions are independent. The force constants $\phi_{\alpha\beta}(\ell,\ell')$ are chosen so as to bring the energy levels of the model system as close as possible to those of our true system. $\vec{u}(\ell,\ell') = \vec{u}(\ell) - \vec{u}(\ell')$. Since the vacancies are independent and randomly located

$$\langle (C_\ell C_{\ell'}) \rangle = \langle C_\ell \rangle \langle C_{\ell'} \rangle = C^2$$

where

$C = \langle C_\ell \rangle_o$ is an average in the states of H_o. The Helmholtz free energy of the model crystal is

$$F_o = F_h - K T \log \frac{(N+n)!}{n!\, N!} - STn \qquad \ldots \quad (3.10)$$

F_h is the usual harmonic free energy corresponding to a system with Hamiltonian H_o. The second term in (3.10) is the configurational entropy of n randomly located vacancies, and S is the local entropy change around an individual vacancy. The last term in (3.10) is normally[9,10] $g = (e + Pv + ST)n$ where g is the free energy of vacancy

formation. We retain only the entropy term here since we ignore all energy changes when vacancies are introduced in our model system. Using the Gibbs-Bogoliubov variational principle the trial Helmholtz free energy of the true system is

$$F_T = F \leq F_o + \langle H - H_o \rangle \quad \ldots \quad (3.11)$$

which is an upper bound to the true free energy. To find the best model force constants $\phi_{\alpha\beta}(\ell,\ell')$ and the thermal vacancy concentration and the relative mean square vibrational amplitude $\Lambda_{\alpha\beta}(\ell\ell') = \langle u_\alpha(\ell\ell')\ \mu_\beta(\ell\ell') \rangle$ [11,12,13] we minimize F_T. At the minimum

$$\delta F_T = \left(\frac{\partial F_T}{\partial \phi_{\alpha\beta}(\ell\ell')}\right)\delta\phi_{\alpha\beta}(\ell\ell') + \left(\frac{\partial F_T}{\partial \Lambda_{\alpha\beta}(\ell\ell')}\right)\delta\Lambda_{\alpha\beta}(\ell\ell') + \left(\frac{\partial F_T}{\partial n}\right)\delta n = 0 \quad (3.12)$$

We treat $\phi_{\alpha\beta}(\ell\ell')$, $\Lambda_{\alpha\beta}(\ell\ell')$ and n as independent variables which means that the coefficients of the differentials in (3.12) must vanish individually. We note that the kinetic energies in equations (3.7) and (3.8) will cancel out since

$$\sum_{\ell}^{N_L} (1 - C_\ell) = N$$

and

$$\sum_{\ell}^{N_L} \langle T_\ell (1 - C_\ell) \rangle_o = \sum_{\ell}^{N_L} \langle T_\ell \rangle_o \langle 1 - C_\ell \rangle_o = N_L \langle T_\ell \rangle_o (1 - C) = N \langle T_\ell \rangle_o$$

$$\langle H - H_o \rangle = \frac{1}{2} \sum_{\ell\ell'}^{N_L} \langle V(r_{\ell\ell'}) \rangle_o (1 - C)^2 - \frac{1}{2} \sum_{\ell\ell'}^{N} \langle V_H(r_{\ell\ell'}) \rangle_o \quad \ldots \quad (3.13)$$

$$= \frac{1}{2} \sum_{\ell\ell'}^{N_L} \{\langle V(r_{\ell\ell'}) \rangle_o (1 - C)^2 - \langle V_H(r_{\ell\ell'}) \rangle_o (1 - C) \quad \ldots \quad (3.14)$$

3.3 DYNAMICS

The model force constants $\phi_{\alpha\beta}(\ell\ell')$ and the relative mean square

vibrational amplitude $\Lambda_{\alpha\beta}(\ell\ell')$ are determined from $\frac{\partial F_T}{\partial \Lambda_{\alpha\beta}(\ell\ell')} = 0$ and $\frac{\partial F_T}{\partial \phi_{\alpha\beta}(\ell\ell')} = 0$. From equation (3.13)

$$\langle H - H_o \rangle = \frac{1}{2} \sum_{\ell\ell'}^{N_L} \langle V(r_{\ell\ell'}) \rangle_o (1 - C)^2 - \frac{1}{2} \sum_{\ell\ell'}^{N} \{\langle V_H(R_{\ell\ell'}) \rangle_o$$

$$- \frac{1}{2} \vec{u}(\ell\ell') \phi_{\alpha\beta}(\ell\ell') \vec{u}_\beta(\ell\ell') \qquad \ldots \quad (3.15)$$

Using the well known result that for any function

$$f(r + u) = e^{u.\nabla} f(r) \qquad \ldots \quad (3.16)$$

the first term on the right hand side of (3.15) can be written as

$$\langle V(r_{\ell\ell'}) \rangle (1 - C)^2 = \langle \exp u_\alpha(\ell\ell').\nabla_\alpha \rangle V(R_{\ell\ell'}) (1 - C)^2 \qquad \ldots \quad (3.17)$$

where $r_{\ell\ell'} = R_{\ell\ell'} + u_{\ell\ell'}$. Invoking the property of harmonic oscillators $\langle e^{x.u} \rangle = e^{[\langle (u.x)^2 \rangle / 2]}$ then

$$\langle H - H_o \rangle = \frac{1}{2} \sum_{\ell\ell'}^{N_L} \{ e^{\frac{1}{2} \vec{\Lambda}_{\alpha\beta}(\ell\ell') \vec{\nabla}_\alpha(\ell\ell') \vec{\nabla}_\beta(\ell\ell')} V(R_{\ell\ell'}) \times (1 - C)^2$$

$$- V(R_{\ell\ell'}) - \frac{1}{2} \vec{\phi}_{\alpha\beta}(\ell\ell') \Lambda_{\alpha\beta}(\ell\ell') \} \qquad \ldots \quad (3.18)$$

Then

$$\frac{\partial F_T}{\partial \phi_{\alpha\beta}(\ell\ell')} = \frac{\partial F_h}{\partial \phi_{\alpha\beta}(\ell\ell')} + \frac{\partial}{\partial \phi_{\alpha\beta}(\ell\ell')} \langle H - H_o \rangle_o = 0 \qquad \ldots \quad (3.19)$$

leads to the usual harmonic relation

$$\Lambda_{\alpha\beta}(\ell\ell') = \frac{\hbar}{MN} \sum_{q\lambda} (1 - e^{i\vec{q}.\vec{R}_{\ell\ell'}}) \vec{\epsilon}_\alpha(q\lambda) \vec{\epsilon}_\beta(q\lambda) \coth (\beta\hbar \omega_{q\lambda}/2) \qquad \ldots \quad (3.20)$$

which holds for pure crystals and those with vacancies. From the second term of equation (3.12) we get

$$\Phi_{\alpha\beta}(\ell\ell') = \langle \nabla_\alpha(\ell\ell') \nabla_\beta(\ell\ell') V(r_{\ell\ell'}) \rangle (1 - C)^2 \qquad \ldots \quad (3.21)$$

These are force constants of the model system which best represent the real crystal. The present SCH theory differs from that developed in chapter 2 in that the force constants are multiplied by a factor $(1 - C)^2$. Aksenov[11] and Adkhamov, Gomovsky and Lebedev,[12] obtain a similar factor $(1 - C)^2$. The average in (3.21) is similar to that in (2.7).

Higher order approximations to the SCP theory can be calculated in the usual way using perturbation theory[13] with $\langle H - H_o \rangle$ in (3.18). The only difference introduced by the vacancies is that the force constants are multiplied by $(1 - C)^2$. Explicitly the cubic coefficient is

$$\phi_{\alpha\beta\gamma}(oo\ell) = \langle \nabla_\alpha(o\ell)\ \nabla_\beta(o\ell)\ \nabla_\gamma(o\ell)\ V(R_{o\ell}) \rangle\ (1 - C)^2 \qquad \ldots \qquad (3.22)$$

3.4 CONCENTRATION OF VACANCIES

To determine the vacancy concentration we use the last term in equation (3.12)

$$\frac{\partial F_T}{\partial n} = \frac{\partial F_o}{\partial n} + \frac{\partial}{\partial n} \langle H - H_o \rangle_o = 0 \qquad \ldots \qquad (3.23)$$

using equation (3.10)

$$\frac{\partial F_T}{\partial n} = K_\beta T \log \frac{n}{N + n} - ST + \frac{\partial c}{\partial n} \frac{\partial}{\partial c} \langle H - H_o \rangle \qquad \ldots \qquad (3.24)$$

Using equation (3.14) and $\frac{\partial c}{\partial n} = \frac{1}{N_L}$ we find

$$C = \frac{n}{N + n} = e^{-(\varepsilon - ST)/K_\beta T} \qquad \ldots \qquad (3.25)$$

where

$$\varepsilon = \left[-\sum_{\ell}^{N_L} \langle V(r_{o\ell}) \rangle_o\ (1 - C) + \frac{1}{2} \sum_{\ell}^{N_L} \langle V_H(r_{o\ell}) \rangle_o \right. \qquad \ldots \qquad (3.26)$$

is the energy of formation of a vacancy. The ε is the energy required to remove an atom from the crystal to the surface. The first term in (3.26) is the loss in potential energy when an atom is removed from the crystal. The second term represents the gain in potential energy when the atom is placed on the surface. If the crystal is under external pressure we must add a pv term to the argument in (3.25), giving $h = \varepsilon + pv$ where v is the vacancy formation volume. In all cases v was taken to be equal to the atomic volume.

3.5 EINSTEIN APPROXIMATION

The Einstein approximation to the SCP theory is done in a way similar to chapter 2. The SCEC equations with vacancies are similar to those already derived except that all the force constants are multiplied by a factor $(1 - C)^2$. The Einstein frequency is

$$\omega^2_E = \sum_\tau' (2\pi\Lambda)^{-3/2} \int d\vec{u}\, e^{-\frac{u^2}{2\Lambda}} \left(\frac{d^2V}{dr^2} + \frac{2}{r}\frac{dV}{dr}\right) \times (1 - C)^2 \quad \ldots \quad (3.27)$$

while the Einstein frequency with the cubic term is

$$\omega^2(SCE + C) = \omega^2_E + 2\omega_E\, \overline{\Delta}(\omega_E) \quad \ldots \quad (3.28)$$

where

$$\overline{\Delta}(\omega_E) = \frac{-2.36\hbar}{12M^2\omega^4_E} [2n(\omega_E) + 1] \sum_\ell' \left(\left\langle \frac{d^3}{dr^3} V(R_\ell + u)\right\rangle\right)^2 \times (1 - C)^4 \quad (3.29)$$

$$\Lambda = \frac{\hbar}{M\omega_E} \coth(\beta\hbar\omega_E/2) \quad \ldots \quad (3.30)$$

The basic self consistency equations in SCEC + V are (3.28), and (3.30)

together with (3.25), (3.27) and (3.29).

The equation of State of the crystals is determined from the Einstein approximation to the ISC theory.[13,14,15] In this approximation the Helmholtz free energy

$$F_{ISCE} = F_{SCE} + \Delta F_3 \qquad \ldots \qquad (3.31)$$

where

$$\frac{F_{SCE}}{N} = \frac{1}{2} \sum_{\ell}{}' \langle V(r_{o\ell}) \rangle_E (1 - C)^2 + 3\beta^{-1} \log(2 \sinh (\beta\hbar\omega_E/2))$$

$$- \frac{3}{4} \hbar\omega_E \coth(\beta\hbar\omega_E/2) + \frac{\beta^{-1}}{(1 - C)} \{C \log C - (1 - C) \log (1 - C)\} - STC$$

$$\ldots \qquad (3.32)$$

and

$$\Delta F_3 = \frac{- 2.36 \hbar^2 (12 n(\omega_E)^2 + 12 n (\omega_E) + 1)}{144 \omega^4_E M^3} \times$$

$$\sum_{\ell}{}' \langle \left(\frac{d^3}{dr^3} V(r_{o\ell})\right)_E \rangle^2 (1 - C)^4 \qquad \ldots \qquad (3.33)$$

The temperature dependence of the crystal volume is determined from solving the equation

$$P = - \left(\frac{\partial F}{\partial V}\right)_T = 0 \qquad \ldots \qquad (3.34)$$

and the isothermal bulk modulus is

$$B_T = -V \left(\frac{\partial^2 F}{\partial V^2}\right)_T$$

The lattice dilation and isothermal bulk modulus will be determined using different pair potentials as a function of temperature.

REFERENCES

(1) W.E. Schoknecht and R.O. Simmons, in Thermal Expansion A.I.P. Conference Proceedings (Ed. M.G. Graham and H.E. Hagy) 3, 169 (1971).

(2) L.A. Schwalbe. Phys. Rev. B14, 1722 (1976).

(3) D.L. Losee and R.O. Simmons. Phys. Rev. 1722,934 (1968).

(4) P.R. Granfors, A.T. Macrander and R.O. Simmons. Phys. Rev. B24, 4753 (1981).

(5) H.R. Glyde. J. Phys. Chem. Sol. 27, 1659 (1966).

(6) H.R. Glyde and J.A. Venables. J. Phys. Chem. Sol. 29, 1093 (1968).

(7) D.R. Squire and W.G. Hoover. J. Chem. Phys. 50, 701 (1969).

(8) K.F. Stripp and J.G. Kirkwood, J. Chem. Phys. 22, 1579 (1954).

(9) A.V. Chadwick and H.R. Glyde in Rare Gas Crystals Vol. II ed. by M.L. Klein and J.A. Venables (Academic Press New York 1977).

(10) C.P. Flynn. Point defects and diffusion (Oxford University Press 1972).

(11) V.L. Aksenov. Sov. Phys. Solid State 14, 1718 (1973).

(12) A.A. Adkhamov, V.A. Gumovskii and V.I. Lebedev. Sov. Phys. Doklady 25, 928 (1981), Rev. Int. Hautes Temper. Refract. Fr. 17, 59 (1980).

(13) H.R. Glyde and M.L. Klein. Crit. Rev. Solid State Sci. 2, 181 (1971).

(14) V.V. Goldman, G.K. Horton and M.L. Klein. J. Low Temp. Phys. 1, 391 (1969).

(15) M.L. Klein and T.R. Koehler, in Rare Gas Crystals, ed. by M.L. Klein and J.A. Venables, Vol. I (Academic New York 1976).

CHAPTER 4

§ Test of ISCE

4.1 Introduction

4.2 Application to Rare Gas Crystals

4.3 Results

CHAPTER 4

4.1 INTRODUCTION

In this chapter we will study some selected thermodynamic properties of the rare gas crystals (RGC's) using the Improved Self Consistent Einstein model. The development of the self consistent phonon theory in the late sixties, resulted in a lot of energy being directed towards studying the dynamic and thermodynamic properties of both alkali halides and RGC's. These have been reviewed by Glyde and Klein.[1] In addition the heavier RGC's have been reviewed exhaustively by Klein and Koehler[2] and helium by Glyde.[3] The agreement between theory and experiment when realistic pair potentials of Bobetic and Barker[4] (BB), Barker, Fisher and Watts[5] (BFW) are used in the determination of the dynamic and thermodynamic properties of Ar and Kr with the ISC theory is excellent.[6-9] The use of the Aziz-Chen[9] (AC) potential in Ar with the SCH + C gives very good agreement for the dispersion curves and the dynamic form factor.[10] The full self consistent phonon theory together with Monte Carlo[11] and molecular dynamics[12] techniques provide excellent tools for studying thermodynamic properties of RCG's, hence we do not expect that an Einstein approximation would be an adequate replacement for the more accurate techniques. However the simplicity of the ISCE makes it attractive in so far as reducing the numerical complications and long computing times in the more accurate techniques. Our aim here is to test the ISCE against the ISC and experiment, since the companion model SCEC is used in the instability of the systems studied. We calculate the temperature dependence of the crystal volume and the isothermal bulk modulus using the Morse potential,

Lennard-Jones potential, and the Aziz-Chen potential for Ar, and for Kr and Xe only the Morse potential.

4.2 APPLICATIONS TO RARE GAS CRYSTALS

In this section we apply the theory outlined in the two previous chapters to calculate lattice dilation and zero pressure bulk moduli as a function of temperature. Our calculations consist of evaluating the Helmholtz free energy F, at a given temperature at five very closely spaced lattice points, and then performing a least square fit to F. We then use the condition $(\frac{\partial F}{\partial V})_T = 0$ to obtain the lattice parameter. The isothermal bulk modulus B_T is then obtained from the same fit using the definition $B_T = -V\,(\frac{\partial^2 F}{\partial V^2})_T$. For Ar we use the AC, the Morse and the Lennard-Jones potentials. In the case of Krypton and Xenon only the Morse potential was used. The AC potential has the following form

$$V(r) = \varepsilon\, V^*(x), \quad x = r/R_M \qquad \ldots \qquad (4.1)$$

$$R_M = 3.75A^o, \quad \varepsilon/K_\beta = 143.224\ K$$

where

$$V^*(x) = Ax^\gamma \exp(-\alpha x) - (\frac{C_6}{x^6} + \frac{C_8}{x^8} + \frac{C_{10}}{x^{10}})\, F(x) \qquad \ldots \qquad (4.2)$$

$$F(x) = \begin{cases} \exp\left[-\left(\frac{D}{x} - 1\right)^2\right] & x < D \\ 1 & x \geq D \end{cases} \qquad \ldots \qquad (4.3)$$

The Morse potential is

$$V(r) = De^{-2\gamma(r - R_o)} - 2De^{-\gamma(r - R_o)} \qquad \ldots \qquad (4.4)$$

where the parameters D, γ, R_o as determined by Glyde[13] are listed in

Table 1. In Ar we also determined the above parameters so that the ISCE model gave the best fit to the observed sublimation energy and compressibility and zero pressure at absolute zero. These are $D = 150.89$ K, $\gamma = 1.685$ Å^{-1}, $R_o = 3.772$ Å using these parameters, the lattice dilation found differed only slightly from that found using Glyde's parameters.

The Lennard-Jones (12.6) potential is

$$V(r) = 4\epsilon \left\{ \left(\frac{\sigma}{R}\right)^{12} - \left(\frac{\sigma}{R}\right)^{6} \right\} \qquad \ldots \qquad (4.5)$$

with the parameters of Horton and Leech[14]

$$\epsilon = 119.8 \text{ K}, \qquad \sigma = 3.405 \text{ Å}.$$

In the case of the Morse potential the force constants' averages can be done analytically. For example the Einstein frequency squared is

$$\omega_E^2 = \frac{2D\gamma^2}{3M} \sum_{\tau}' \frac{n(\tau)}{\tau} \left\{ 2\left(\tau - 2\gamma\Lambda - \frac{1}{\Lambda}\right) \exp\left[2\gamma^2\Lambda - 2\gamma(\tau - R_o)\right] \right.$$

$$\left. - \left(\tau - \gamma\Lambda - \frac{2}{\Lambda}\right) \exp\left[\left(\gamma^2 \frac{\Lambda}{2}\right) - \gamma(\tau - R_o)\right] \right\} \qquad \ldots \qquad (4.6)$$

The averaged third derivative in the Einstein approximation is

$$\left\langle \frac{d^3}{dV^3} V(R + u) \right\rangle_E = 2\gamma^3 D \left\{ 4(\tau - 2\gamma\Lambda) \exp\left[2\gamma^2\Lambda - 2\gamma(\tau - R_o)\right] \right.$$

$$\left. - (\tau - \gamma\Lambda) \exp\left[\left(\gamma^2 \frac{\Lambda}{2} - \gamma(\tau - R_o)\right)\right] \right. \qquad \ldots \qquad (4.7)$$

the averaged potential is

$$\frac{1}{2}\sum_{\ell}{}' \langle V(r_{o\ell})\rangle = \frac{D}{2}\sum_{\tau}{}' n(\tau)\ \{\exp\ [2\gamma^2\Lambda - 2\gamma(\tau - R_o)]$$

$$x\ (1 - \frac{2\gamma\Lambda}{\tau}) - \exp\ [\frac{\gamma^2\Lambda}{2} - \gamma(\tau - R_o)]\ x\ (1 - \frac{\gamma\Lambda}{2\tau})\} \qquad \ldots \qquad (4.8)$$

Λ is given by equation (3.30).

4.3 RESULTS

The results of the temperature dependence of the lattice dilation in the present ISCE model, the ISC calculation and the observed values are displayed in fig. 1. The ISC (BB) is the Improved Self Consistent theory calculation[2] using the Bobetic-Barker[4] potential. It is the most accurate analytical calculation of $\frac{\Delta L}{L_o}$ to date, and any analytical calculation should aim to reproduce its results. From the figure we see that ISC (BB) $\frac{\Delta L}{L_o}$ is in best agreement with observed values for Ar. Shown on the same figure for Ar are ISCE (LJ) calculated with the Lennard-Jones potential using the ISCE model, ISCE (Morse) with ISCE model using the Morse potential, and ISCE (AC) with the ISCE model using the Aziz-Chen potential. To date the most accurate Ar-Ar pair potential is the Aziz-Chen potential, unfortunately there are no calculations of either the temperature dependence of the lattice dilation or the isothermal bulk modulus with the ISC model, so all theoretical calculations are compared with the ISC (BB) calculation. The Bobetic-Barker potential is accurate enough, so for the present calculations of the bulk thermodynamic properties we regard it as essentially indistinguishable from the Aziz-Chen potential.

There is a large discrepancy between the ISCE (AC) curve and the experiment at high temperature, this is attributable to the deficiency of the ISCE model. The ISCE (LJ) curve lies closest to the ISC (BB) and experimental curves. This agreement is somewhat misleading, because the Lennard-Jones potential is not an accurate Ar-Ar potential. This agreement can be ascribed to a fortuitous cancellation of errors made in the use of the Lennard-Jones potential in the calculation of the Helmholtz free energy using the ISCE model. A similar agreement in the lattice constant in Ar, Kr and Xe has been found by Paskin and[15] his co-workers using an analytical model, apparently similar to the ISCE model called the Self Consistent Averaged Phonon theory (SCAP). Their agreement is even more artificial because they adjusted the Lennard-Jones potential parameters to give the correct sublimation energy and compressibility and zero pressure at absolute zero. The agreement in this case is also a cancellation of errors since the ISCE and SCAP are very similar approximations.

In the same figure is the ISCE (Morse) calculated with the Morse potential with parameters determined by Glyde.[13] A calculation performed with the Morse potential parameters given in 4.2 results in a curve lying between the ISCE (LJ) and ISCE (Morse) very close to the ISCE (Morse). The curve was left out to avoid clutter, besides all calculations investigating crystal stability are done using Glyde's[13] parameters. In Xe the same discrepency as in Ar between ISCE (Morse) curve and experiment is found. The ISCE (Morse) curve in Kr happens to agree well with experiment.

In figure 2 we display the zero-pressure isothermal bulk modulus B_T vs. temperature. The ISC (BB) 3-body calculation is in

excellent agreement with experiment. The ISCE (Morse) is in reasonable agreement with experiment, but there are some clear discrepancies. As in figure 1 the ISCE (AC) shows the largest discrepancy, while the ISCE (LJ) is in best agreement with experiment. Again for the Aziz-Chen potential the disagreement represents the shortcomings of the ISCE model, and the apparent agreement with the Lennard-Jones potential curve is due to cancellation of errors as before. The vacancies were found to have very little effect on the $\frac{\Delta L}{L_o}$ and B_T calculated in the ISCE model up to the triple point. But for temperatures just below the instability they do affect bulk thermodynamic properties. From figures 1 and 2 we see that the ISCE does not give very accurate thermodynamic properties for the rare gas crystals, hence there will be some errors in the equation of state calculated with this model. All lattice parameters used in stability studies were determined using the ISCE with the Morse potential, since the ISCE is the companion approximation of the SCEC theory. For the purpose of our stability studies the lattice parameters from ISCE (Morse) are reasonable enough. The experimental curves/points in figures 1 and 2 are from references (16-22).

REFERENCES

(1) H.R. Glyde and M.L. Klein. Crit. Rev. Solid State Sci. 2, 181 (1971).

(2) M.L. Klein and T.R. Koehler, in Rare Gas Solids, ed. by M.L. Klein and J.A. Venables (Academic, New York 1976), Vol. I, Chapter 6.

(3) H.R. Glyde, in Rare Gas Solids, ed. by M.L. Klein and J.A. Venables (Academic, New York 1976), Vol. I, Chapter 7.

(4) M.V. Bobetic and J.A. Barker. Phys. Rev. B2, 4169 (1970).

(5) J.A. Barker, R.A. Fisher and R.O. Watts. Mol. Phys. 21, 657 (1971).

(6) J.A. Barker, M.L. Klein and M.V. Bobetic. Phys. Rev. B2, 4176 (1970).

(7) M.L. Klein, J.A. Barker and T.R. Koehler. Phys. Rev. B4, 1983 (1971).

(8) M.V. Bobetic, J.A. Barker and M.L. Klein. Phys. Rev. B5, 3185 (1972).

(9) R.A. Aziz and H.H. Chen. J. Chem. Phys. 67, 5719 (1977).

(10) H.R. Glyde and M.G. Smoes. Phys. Rev. B22, 6391 (1980).

(11) M.L. Klein and R.D. Murphy. Phys. Rev. B6, 2433 (1972).
J.A. Barker and M.L. Klein. Phys. Rev. B7, 4707 (1973).

(12) See Ref. 2.

(13) H.R. Glyde. J. Phys. C3, 810 (1971).

(14) G.K. Horton and J.W. Leech. Proc. Phys. Soc. 82, 816 (1963).

(15) A. Paskin, A.M. Llois de Kreimer, K. Shukla, D.O. Welch and G.J. Dienes. Phys. Rev. B22, 1297 (1982).

(16) O.G. Peterson, D.N. Batchelder and R.O. Simmons. Phys. Rev. 150, 703 (1965).

(17) D.L. Losee and R.O. Simmons. Phys. Rev. 172, 1944 (1968).

(18) J.V. Trefny and B. Serin. J. Low Temp. Phys. 1, 231 (1969).

(19) M.S. Anderson and C.A. Swenson. J. Chem. Phys. Sol. 36, 145 (1975).

(20) A.O. Urvas, D.L. Losee and R.O. Simmons. J. Phys. Chem. Sol. 28, 2269 (1967).

(21) P. Korpium and H.J. Coufal. Phys. Stat. Sol. (a) 10, 187 (1971).

(22) P. Korpium, W. Albrecht, T. Müller and E. Lüscher. Phys. Lett. 48 A, 253 (1974), see also ref. 19.

CHAPTER 5

CHAPTER 5

5.1 INTRODUCTION

In this chapter we apply the theory developed in chapters 2 and 3 to investigate the stability of crystals against large vibrational amplitude. In section 5.2 we use the full SCH, SCH + cubic approximations, the SCE and the SCEC models to investigate the stability of RGC's. To model the RGC's we represent the pair interaction by the Morse potential. The merit of using the Morse potential is that integrals in the averages can be done analytically and as we saw in the previous chapter it is a reasonable enough potential for present needs only. The averages have already been given in chapter 4, see equations (4.6), (4.7) and (4.8), and will not be repeated here.

5.2 STABILITY OF IDEAL RGC's USING THE SCP THEORY

For the purposes of this section we set the volume of the RGC's at those observed for temperatures below melting. These were taken from Peterson et al,[1] Batchelder et al,[2] Losee and Simmons,[3] and Trefny and Serin[4] for Ne, Ar, Kr and Xe respectively. For temperatures above the observed melting temperatures we arbitrarily set the volume at the observed melting volume. An alternative to this would have been to arbitrarily extrapolate the volume to higher temperatures. However we felt that for the purpose of comparing the approximations, keeping the volume fixed at the observed melting volume was adequate. The instability temperatures of the RGC's predicted by the different models are listed in Table 2. The SCH and SCE models as expected from previous

work[5-8] are found to be very stable and predict T_I about 300 times the observed melting temperatures. The instability temperatures are almost the same for the SCH and SCE models. This is consistent with the results in the Wigner solid[9-10] where the SCH and SCE instability temperatures are the same.

The T_I predicted by the SCH + C is much lower, but still 4 times the observed T_M. The cubic anharmonic term equation (2.25) is always negative and reduces the phonon frequencies. It therefore makes the crystal less stable. The SCH + C is the most complete and accurate model used here. The T_I for the SCE + C model, where we made an Einstein approximation to both the harmonic and the cubic terms, are nearly the same as, but 5% higher than the SCH + C values.

In the last model in Table 2, denoted SCEC, the cubic term in the Einstein approximation is included in the iteration procedure, rather than simply added as a perturbation, a procedure already described in (2.6). We multiply the cubic shift by a single numerical constant in order that the SCEC model has the same instability temperature for Ar as the complete SCH + C. Clearly, the SCEC and SCH + C models continue to give the same T_I for the other RGC's. Again in Table 2, while the SCEC model leads to a somewhat lower T_I, there is little difference from SCE + C model where the cubic term is simply addes as a perturbation.

In Table 3 we show the reduced vibrational amplitude δ at T_I calculated for different approximations. The T_I itself differs for different approximations. The δ_I (SCEC) is substantially smaller than δ_I (SCH) and δ_I (SCE) because the instability temperature T_I is much lower in the SCEC case. The δ_I values are however unreliable because they come from models that are deficient. The most detailed calculations

of δ at melting[11,12] find δ = 0.15–0.17 for thermal melting and δ = 0.32–0.35 for quantum melting.

To display the nature of the instability we go back to the simplest SCE model. In fig. 3 we plot ω^2_E/ω_o^2 versus the reduced vibrational amplitude δ; where ω^2_E is given by equation (2.15), δ given by (2.16) and ω_o^2 is the static crystal vibrational frequency squared given by (2.15) with $\Lambda = 0$. The example is Ar fixed at the observed melting volume. As δ increases from zero, ω^2_E increases to a maximum at $\delta \simeq 0.29$. For $\delta \geq 0.29$, there is no self consistent solution, and ω^2_E continues to decrease when (2.15) and (2.16) are iterated until negative ω^2_E are reached. Thus at $\delta = 0.29$ ω^2_E goes discontinuously to negative values signalling an unstable crystal.

In fig. 4 we plot the Helmholtz free energy vs. δ in SCE for Ar. This shows that F_{SCE} ceases to have a minimum at any δ for $T \geq T_I$.

In the most complete SCH + C model the instability occurs because some specific phonon mode frequencies, given by the position of the maximum in the response function (2.17), go to zero or below. We found the transverse modes along [110] and [111] directions having small reduced wave vectors in the region $q \lesssim (0.1, 0.1, 0)$ and $q \lesssim (0.1, 0.1, 0.1)$ become unstable first. We checked at very low wave vectors, but these phonons had similar stability to those somewhat further out from the zone centre. In fig. 5 we show the temperature dependence of $T_1[q, -q, 0]$ branch phonons for $q = 0.01$, 0.05 and 0.1 for Ar at a fixed volume ($V = 24.3$ cm^3/mole). We see that the phonon frequencies in the region $q \lesssim 0.1$ show the largest temperature dependence leading to a very flat T_1 dispersion curve in this q region near the instability temperature.

The phonons near $q \approx 0.1$ appeared to be least stable at T_I, the position of the peak in the response function (2.17) dropped discontinuously to zero (or below).

The temperature dependence of the frequency ω^2 (SCEC) in the SCEC model is shown in fig. 6. The ω^2_o is the static value at T = 0 K calculated from (2.24), setting the vibrational amplitude $\Lambda = 0$. Between T = 0 and T = 83 K when the crystal is expanding ω^2 (SCEC) decreases. Above T = 83 K the volume is held constant at the observed value at melting for Ar, and ω^2 (SCEC) increases until it becomes unstable at 380 K. Again as in the SCE model there is no precursor to the instability.

The steepness of the hard core in the Morse potential is set by the parameter γ in equation (4.4). To test the dependence of T_I on the steepness of the hard core we arbitrarily varied γ for Ar (around the best value $\gamma = 1.55$ for SCH) from 1.1 to 2.05. The other parameters D and R_o were recalculated for each γ to fit the sublimation energy L_o and reestablish zero pressure at T = 0 K. These parameters are given in Table 4. The dependence of T_I for SCE and SCH models on γ is displayed in Table 5. We see that T_I increases as γ is increased. This is to be expected and is reasonable since the crystal becomes stiffer and the frequencies increase as γ increases. It is also interesting that the SCH and SCE models predict T_I closer together as γ increases. This is probably because T_I is high and the crystal completely classical, though it is not clear. In the one component plasma (OCP) the SCH and SCE models give identical T_I within a few percent in both the classical and quantum limit.[7]

5.3 STABILITY OF RGC's WITH VACANCIES

In chapter 4 we determined the lattice parameter a(T, P) as a function of temperature and pressure using the ISCE free energy plus vacancies given by (3.31). With the lattice parameters determined, the crystal temperature was increased in steps and the SCEC frequency (3.28), and vacancy concentration (3.25) was determined at each temperature. Eventually a temperature was reached at which no self consistent solution in the SCEC with vacancies was found. This is the instability temperature T_I. The zero pressure instability temperatures, the vacancy concentrations just before instability, the reduced vibrational amplitudes are displayed in Table 6. We see that T_I lies about 40% above the observed melting temperature T_M, and the vacancy concentrations range from 2.5% to 4%. The Lindemann ratios δ of approximately 0.16, which happen to agree with accurate determinations in more accurate calculations at T_M, are a result of a cancellation of two errors; the Einstein approximation predicts δ to be too small and T_I lies above T_M. We note that the T_I calculated here is an instability temperature and lies above T_M as in simulation studies.[12]

In this study, the creation of vacancies plays the role of removing atoms from the crystal interior and placing them on the surface. This results in the reduction of the force constants between atoms adjacent to vacant sites, and also in the reduction of the interaction potential seen by these atoms. Consequently, the creation of more vacancies becomes easier. The reduced force constants result in smaller ω^2_E (SCEC) which leads to larger root mean square vibrational amplitudes of the atoms. The vacancies only play a key role near the

instability temperature where their numbers are significant. At lower temperatures the amplitudes are only a result of the dynamics.

In fig. 7 we display the temperature dependence of the square of the SCEC frequency for Ar, Kr and Xe. At low temperatures the decrease in ω^2 (SCEC) is slow, but as the lattice dilates the rate of decrease increases. As T approaches T_I ω^2 (SCEC) decreases sharply until it falls discontinuously to negative unstable values, where the self consistent equations in the SCEC + V model cease to have solutions. As seen in figures 3, 6 and 7, the square of the frequencies falls discontinuously to unstable values; the sudden loss of crystal stability is characteristic of first order phase transitions.

In fig. 8, we show the pressure dependence of the instability temperatures for Ar, Kr and Xe. Also shown are the experimental melting curves of Daniels et al[13,14] for Ar and Kr and for Xe from Stryland et al.[15] As the applied pressure increases, the ratio of T_I to T_M increases. In Ar and Kr this ratio goes from about 1.4 at zero pressure to about 1.5 at 5 Kb. This increase is a result of the increase in the error made in predicting the crystal volume as the external pressure increases. Consequently we attach no physical significance to it. The triangle in fig. 8 for Ar is the zero pressure instability temperature determined with the Aziz-Chen potential. The T_I here is about 1.6 times T_M for Ar. The reason for this is that the ISCE + V model, as seen in fig. 1 predicts a lower equilibrium volume with the Aziz-Chen potential. In general, the smaller the volume predicted by the model, the higher the instability temperature goes. The ISCE + V model gives a smaller volume than observed with the Morse potential at zero pressure, and it is even lower as pressure

increases, hence the increase in the ratio T_I/T_M as depicted by fig. 8.

In fig. 9 we show the calculated vacancy concentration in Ar, Kr and Xe versus $\frac{1}{T}$. The calculated vacancy concentration C in Ar lies close to the Monte Carlo calculation of Squire and Hoover.[16] In Kr the calculated C lies between Monte Carlo[16] results and experimental concentrations.[17] In Xe at T_M the calculated concentration C also lies well below the observed C.[18] In Table 7 we show the calculated vacancy formation enthalpy h(T). Clearly the calculated h(T) at T_M lies above the observed values. This is a well known and unresolved problem for RGC's. The point is very clearly discussed by Chadwick and Glyde[19] and shall not be dwelt on at length here. The model used here predicts fewer vacancies than observed and larger h(T) than observed in Kr and Xe. The calculated values of h(T) are consistent with those calculated using a variety of pair potentials as clearly discussed in Ref. 19. We find that h(T) depends on temperature. For example h(T) drops from 857 K at T = 83 K to 705 K at T = 110 K in Ar. In all calculations the observed values $S = 2K_\beta$ were used.[18,19]

5.4 STABILITY OF THE LENNARD-JONES SYSTEM

In this section we use the SCEC + V model to determine the instability densities ρ_I, in a classical system of particles interacting via a Lennard-Jones potential.

$$V(r) = 4\varepsilon \left\{ \left(\frac{\sigma}{r}\right)^{12} - \left(\frac{\sigma}{r}\right)^{6} \right\}$$

We make a comparison with the Monte Carlo simulations of

Hoover and Ross[22] and Street and his co-workers.[23] We consider the same system with mass M = 40 amu, and potential parameters ϵ = 119.86 K and σ = 3.405 Å chosen to simulate Ar. The SCEC + V calculations were done along three isotherms T = 127 K, T = 140 K and T = 328 K. In the Monte Carlo studies at the temperatures above the crystal was observed to break up into a fluid at densities ρ_I smaller than the melting densities ρ_M. The ρ_M was obtained by Hansen and Verlet[24] from determining the Gibb's free energy of the solid and of the fluid and equating them under conditions of equal temperature and pressure.

In Table 8 we list the melting density ρ_M, the Monte Carlo ρ_I (MC), and the SCEC + V instability density ρ_I (SCEC + V) calculated with the Lennard Jones potential. We see from the table that ρ_M's range from 1.16 to 1.25 times ρ_I (SCEC) with the higher ratios applying at high temperatures. The higher ratio at a higher temperature probably reflects the increasing error in pressure and density predicted by the ISCE model as T increases. The Monte Carlo ρ_I and SCEC + V ρ_I are essentially similar, thus suggesting that the vibrational model with point defects may contain the necessary ingredients that lead to crystal instability at high temperatures.

5.5 STABILITY OF THE GAUSSIAN CORE MODEL (GCM)

A: Introduction

In a series of papers Stillinger and Weber[25-27] have carried out a careful molecular dynamics (MD) study of a system of N classical particles interacting via a pairwise repulsive Gaussian potential,

$$\phi(r_{ij}) = \phi_o \exp\left[-\left(\frac{r_{ij}}{\ell}\right)^2\right] \quad \ldots \quad (5.1)$$

In particular, they studied transitions into bcc and fcc structures at absolute zero, melting and freezing. The GCM is very interesting because at high density it shows waterlike properties; i.e. melting under pressure, negative thermal expansion and negative melting volumes. Also the crystalline phase exists only over a finite density range. It is also interesting that at low temperatures the GCM melts at low and high densities. The MD simulations provide an excellent bench mark for testing the simple SCEC + vacancies instability model. We compare the SCEC + V instability T with the MD instability and melting temperatures of Stillinger and Weber.

In the classical limit the GCM can be conveniently described in reduced units. In this limit the equations of motion become universal and independent of M, ϕ_o and ℓ. In reduced units, the length is $X = r/\ell$, density $\rho^* = \rho\ell^3$, temperature $T^* = K_\beta T/\phi_o$, vibrational frequency $\omega^*_E = \omega_E/(\phi_o/m\ell^2)^{1/2}$, and the reduced vibrational amplitude $\lambda^* = \lambda/\ell^2 = 2\langle u_\alpha^2\rangle/\ell^2$. The density range considered by Stillinger and Weber is $0.1 \leq \rho^* \leq 1.0$, where for $\rho^* \leq 0.18$ the crystal is fcc, and bcc at higher densities. We examined both phases, but here we only discuss the bcc phase because it exists over a wider range of densities. In the quantum regime, however, the mass M, the potential depth ϕ_o and the length ℓ must be specified. To study the GCM in the quantum limit we selected M = 40 amu to simulate Ar. The Ar parameters are found to be

$$\phi_o = 848.86 \times 10^3 \text{ K}$$

$$\ell = 1.192 \text{ Å}$$

and for Ne with mass 20 amu the parameters are

$$\phi_o = 258.61 \times 10^3 \text{ K}$$

$$\ell = 0.964 \text{ Å}$$

With this choice of parameters, for $\rho^* = 0.2$ in Ar the external pressure is extremely high, in excess of 5 megabars. The transition from fcc to bcc at $\rho^* = 0.18$ closely resembles a similar transition from fcc to bcc observed in solid helium under extreme pressure.[28,29] With the Gaussian potential (5.1) the integrals in the averages in equations (3.27) and (3.33) can be done analytically. The reduced frequency squared is

$$\omega^{*2}_E = \sum_{\tau^*}{}' \frac{2}{(2\lambda^* + 1)^{3/2}} \left\{ \frac{2}{2\lambda^* + 1} \left[\lambda^* + \frac{(\tau^*)^2}{3(2\lambda^* + 1)} \right] - 1 \right\} X$$

$$\exp\left(\frac{-(\tau^*)^2}{2\lambda^* + 1} \right) \qquad \ldots \qquad (5.2)$$

where

$$\lambda^* = \frac{\hbar}{M\omega_E \ell^2} \coth\left(\frac{\hbar\omega_E}{2K_\beta T} \right)$$

reduces to

$$\lambda^* = 2T^*/(\omega^*_E)^2 \qquad \ldots \qquad (5.3)$$

In the classical limit for $\frac{\hbar\omega_E}{K_\beta T} << 1$. When the cubic anharmonic term is added the frequency is

$$\omega^{*2} = (\omega^*_E)^2 + 2\omega^*_E \overline{\Delta}(\omega^*_E) \qquad \ldots \qquad (5.4)$$

where

$$\overline{\Delta}(\omega^*_E) = \frac{-2.36T^*}{6(\omega^*_E)^5} \sum_{\tau^*}{}' \left\langle \frac{d^3}{dx^3} \Phi(x) \right\rangle_{\tau^*} \qquad \ldots \qquad (5.5)$$

$$\text{and } \left\langle \frac{d^3}{dx^3}\phi(x)\right\rangle = \int_{\tau^*}^{} (2\lambda + 1)^{-5/2} \left[\frac{12\lambda^*(2\lambda^* + 1)}{\tau^*} - \tau^* - \frac{24\lambda^{*2}}{\tau^*}\right.$$

$$\left. + 8\tau^* - 8\tau^{*3}\right] \exp\left[-\frac{(\tau^*)^2}{(2\lambda^* + 1)}\right] \quad \ldots \quad (5.6)$$

here $\tau^* = \tau/\ell$ is the reduced neighbour distance. Equations (5.2), (5.3) and (5.4) constitute the self consistency equations in the SCEC model for the GCM without vacancies.

B: Gaussian Core Model with Vacancies

To include vacancies in the GCM, equations (5.2) and (5.6) are multiplied by the same factors $(1-C)^2$ and $(1-C)^4$, respectively, as in chapter 3. To calculate the vacancy concentration we go back to equation (3.26)

$$C = e^{-(\varepsilon - ST)/K_\beta T} \quad \ldots \quad (5.7)$$

where

$$\varepsilon = h + PV.$$

In reduced units

$$h^* = h/\phi_o$$

$$S^* = S/K_\beta$$

$$P^* = P\ell^3/\phi_o \quad \ldots \quad (5.8)$$

hence

$$C = e^{-(h^* - S^*T^* + P^* v^*)/T^*} \quad \ldots \quad (5.9)$$

where P^* can be found by differentiating the reduced Helmholtz free energy with respect to reduced volume. Here we use the same expression for h as in the case of RGC's, equation (3.26), and v^* is equal to

reduced one atomic volume. Below we derive an approximate expression for S^* since no observed values are available. To estimate S we go back to the definition

$S \equiv$ entropy of a crystal having one vacancy - entropy of a perfect crystal

$= S_V - S_o$

In the SCH approximation the entropy

$$S_o = -\frac{\partial F_h}{\partial T} = K_\beta \left[\sum_{q\lambda} \left(\frac{\hbar\omega^o_{q\lambda}}{2K_\beta T} \coth \left(\frac{\beta\hbar\omega^o_{q\lambda}}{2}\right)\right)\right.$$

$$\left. - \sum_{q\lambda} \log \left(2 \sinh \left(\frac{\beta\hbar\omega^o_{q\lambda}}{2}\right)\right)\right] \quad \ldots \quad (5.10)$$

In the high temperature limit

$$S_o = K_\beta \left[\sum_{q\lambda} \alpha^o_{q\lambda} \left(\frac{1}{\alpha_{q\lambda}}\right) - \sum_{q\lambda} \log (\alpha^o_{q\lambda})\right] \quad \ldots \quad (5.11)$$

$$= K_\beta \left[3N - \sum_{q\lambda} \log (\alpha^o_{q\lambda})\right] \quad \ldots \quad (5.12)$$

where

$$\alpha_{q\lambda} = \beta\hbar\omega_{q\lambda}/2$$

Similarly

$$S_V = K_\beta \left[3N - \sum_{q\lambda} \log (\alpha^V_{q\lambda})\right] \quad \ldots \quad (5.13)$$

$$\therefore S_V - S_o = -\left[K_\beta \sum_{q\lambda} \log (\alpha^V_{q\lambda}) - K_\beta \sum_{q\lambda} \log (\alpha^o_{q\lambda})\right]$$

$$= K_\beta \log \{\pi_{q\lambda} \omega^o_{q\lambda} / \pi_{q\lambda} \omega^V_{q\lambda}\} \quad \ldots \quad (5.14)$$

$$= K_\beta \log \{\pi_{q\lambda} [\omega^o_{q\lambda} / \omega^V_{q\lambda}]\} \quad \ldots \quad (5.15)$$

But we know that

$$\omega^2_{q\lambda} \alpha \langle \nabla_\alpha(\ell\ell') \nabla_\beta(\ell\ell') V(r_{\ell\ell'}) \rangle (1 - C)^2$$

$$\alpha \langle \nabla_\alpha(\ell\ell') \nabla_\beta(\ell\ell') V(r_{\ell\ell'}) \rangle \quad \ldots \quad (5.16)$$

$$\therefore S_V - S_o = K_\beta \log \{(1 - C)^{-3N}\}$$

$$= -3N K_\beta \log (1 - C)$$

$$= 3N K_\beta C$$

Hence the local entropy per vacancy is

$$(S_V - S_o)/n = 3N K_\beta C/n$$

$$= 3K_\beta$$

Many accurate calculations give $S = 2K_\beta - 2.5K_\beta$.[19] The reduced entropy $S^* = 3$ is used in GCM calculations. The instability of the GCM with vacancies is determined by iterating equations (5.2), (5.3), (5.4) and (5.9) with (5.2) and (5.4) multiplied by $(1 - C)^2$ and $(1 - C)^4$ respectively. We note that here we have used the same factor 2.36 in the cubic anharmonic term as in the RGC's.

RESULTS

In Table 9 we display the selected instability temperatures at reduced densities $\rho^* = 0.2, 0.4$ and 1.0 for the SCE and SCEC models. These are compared with the MD instability temperatures and the MD melting temperatures. Clearly the cubic term is very significant and reduces T_I^* substantially. There was very little difference in T_I^*

when the cubic term was iterated rather than added as a perturbation. In fig. 10 we display the instability curve T_I^* versus the inverse reduced density $1/\rho^*$ for bcc GCM crystal calculated using the SCEC model. The continuous line is the SCEC model calculation, also shown are the MD instability and melting temperatures of Stillinger and Weber. On the left hand side of the figure, T_I^* (SCEC) drops dramatically, with pressure melting setting in the region $\rho^* \approx 1.0$. The T_I^* (MD) are the maximum temperatures to which the bcc crystal could be "superheated". There is also a dramatic decrease in T_I^* (MD) and T_M^* (MD) on the left hand side of the figure around $\rho^* = 1.0$. On the figure QL marks the SCEC + V instability volume in the quantum limit calculated with the GCM set to simulate Ar. H represents the instability volume in the harmonic approximation.

Two points are of interest here; firstly, since the pressure is so high at the densities considered here, the vacancy concentration is negligible (see Table 10). This is because the P^*V^* term in equation (5.9) is so large that C is negligible. No apparent vacancy content was observed by Stillinger and Weber. Consequently, the dynamics is entirely responsible for the instability in the SCEC + V for the GCM. It is interesting that here where vacancies are essentially absent a reasonable agreement for T_I^* with direct simulation can be obtained when only the vibrational dynamics contributes. Secondly, the instability temperatures T_I^* found in the MD simulation may be only a limit to superheating and not necessarily the true instability temperature of the crystal. Stillinger and Weber suggest that when the crystal melts a latent heat must be supplied. Since their simulation was done at constant energy, they found they had to raise the crystal

temperature high enough so that after this latent heat was supplied, and the temperature of the system fell, it did not fall below the equilibrium T_M^* at which the fluid could exist. Hence the T_I^* observed in the MD simulation may be set by energy requirements and may not represent the ultimate instability temperature of the crystal at all. The true instability temperature may be higher, thus bringing it closer to SCEC T_I^*.

In fig. 11 we display the Lindemann ratio $\delta(T)$ as calculated in the SCEC model at a reduced density $\rho^* = 0.2$ as a function of reduced temperature. This is compared with the MD values of Stillinger and Weber. In both the MD and SCEC models the δ at the instability temperatures is approximately 0.20, compared to $\delta(T_M^*) = 0.16$. In the SCEC model δ is given by

$$\delta^2 = \frac{3T^*}{[R^* \omega^*_E (SCEC)]^2}$$

in the classical limit. In fig. 12 we show ω^{*2} (SCEC) vs. T^*. As with similar figures for the RGC's the decrease is greater near T_I^* and ω^2 goes discontinuously to negative unstable values at T_I^*.

Before discussing the quantum limit results, we note that we may understand the "pressure melting" of the GCM at high density in the simple Einstein approximation. The Einstein frequency is proportional to $[\frac{d^2V(r)}{dr^2} + \frac{2}{r}\frac{dV(r)}{dr}]$. We see from fig. 13 that $\frac{dV}{dr}$ is always negative. When r is small $\frac{d^2V}{dr^2}$ is also negative thus giving a negative ω^2_E and an unstable crystal at high density. At $r = \ell/2$, $\frac{d^2V}{dr^2}$ becomes positive and at $r = (\frac{3}{2})^{1/2} \ell$ the total force constant, $[\omega^2_E]$ becomes positive. In this simple picture, and assuming nearest neighbour forces, a positive

ω_E^2 and a stable crystal is expected for $\rho^* \leq 0.707$ only. This compares well with $\rho^* \leq 2$ found in the SCEC model for Ar (M = 40 amu). Physically, the Gaussian core potential becomes soft when the particles are very closely packed with nearest neighbour distance $r_{ij} \sim \ell$. The Wigner solid also melts under pressure because the coulomb potential is soft.(9) Also at low density $\rho^* \geq 0.1$ where $r_{ij} >> \ell$ the Gaussian potential acts more like a hard core potential for particles encountering each other. If the temperature is high enough we get thermal melting at low density in the usual way as in hard core systems. As already noted in the quantum limit the mass M, ϕ_o and ℓ need to be specified. Thus in this limit ρ_I^* at which the GCM becomes unstable will depend explicitly on M. We list the pressure melting ρ^* at absolute zero for M = (40, 20 and 5) amu in Table 11. For the mass M = 40 amu, ϕ_o and ℓ were chosen so that the GCM simulated Ar, while for M = 20 amu and 5 amu ϕ_o and ℓ were chosen to simulate Ne. We found that when ϕ_o and ℓ were chosen to simulate He the GCM was unstable for all ρ^*. It is interesting that the Lindemann ratio δ in the quantum limit instability is very small in the GCM. This is because the GCM is under extreme pressures and the RMS vibrational amplitudes are very small. Apparently, if the RMS amplitude (or Lindemann ratio) is small in the crystal, the crystal can "melt" with small Lindemann ration in the quantum limit. This is in contrast to the Wigner electron solid where δ is large at quantum melting. In bcc helium the RMS vibrational amplitude is always large so it follows that δ must be large at quantum melting for solid helium. The results of Table 11 suggest that there is no Lindemann rule for melting in the quantum limit. The δ can take any value at instability or melting. This suggests that Lindemann's rule is not related to intrinsic instability

in a crystal structure. Rather Lindemann's rule holds only for thermal melting in the classical limit. This suggests that the Lindemann's rule reflects the structural dependence of the free energy of the solid relative to that of the fluid. This is, at a critical δ, the free energy of the solid becomes higher than that of the fluid, approximately independently of the interatomic potential.

Finally in Fig. 14 we show the SCH frequency dispersion curves for the GCM, and the Aziz-Chen potential for $\rho^* = 0.2$. These curves look the same as those of other fcc crystals e.g. Ar,[28] except that the energies are high.

REFERENCES

(1) O.G. Peterson, D.N. Batchelder and R.O. Simmons. Phys. Rev. 150, 703 (1966).

(2) D.N. Batchelder, D.L. Losee and R.O. Simmons. Phys. Rev. 162, 767 (1967).

(3) D.L. Losee and R.O. Simmons. Phys. Rev. 172, 944 (1968).

(4) J.U. Trefny and B. Serin. J. Low Temp. Phys. 1, 231 (1969).

(5) T. Matsubara, Y. Iwase and A. Momokita. Prog. Theor. Phys. Jpn. 58, 1102 (1977).

(6) M. Hasegawa, K. Hashimo and M. Watabe. J. Phys. F 10, 619 (1980).

(7) P.M. Platzmann and H. Fukuyama, Phys. Rev. B10, 3150 (1974).

(8) H. Fukuyama and P.M. Platzmann. Solid State Commun. 15, 617 (1974).

(9) H.R. Glyde and G.H. Keech. Ann. Phys. (New York) 127, 330 (1980).

(10) R.C. Albers and J.E. Gubernatis. Phys. Rev. B23, 2783 (1981).

(11) W.L. Slatterly, D.G. Doolen and H.E. DeWitt, Phys. Rev. A21, 2087 (1980), E.L. Pollock and J.P. Hansen, ibid. 8, 3110 (1973).

(12) F.H. Stillinger and T.A. Weber, Phys. Rev. B22, 3790 (1980) and references therein.

(13) W.H. Hardy II, R.K. Crawford and W.B. Daniels. J. Chem. Phys. 54, 1005 (1975).

(14) R.K. Crawford and W.B. Daniels. J. Chem. Phys. 55, 5651 (1971).

(15) J.C. Stryland, J.E. Crawford and M.A. Mastoor. Can. J. Phys. 38, 1546 (1960).

(16) D.R. Squire and W.G. Hoover, J. Chem. Phys. 50, 701 (1969).

(17) D.L. Losee and R.O. Simmons. Phys. Rev. 172, 934 (1968).

(18) P.R. Granfors, A.T. Macrander and R.O. Simmons. Phys. Rev. B24, 4753 (1981).

(19) A.V. Chadwick and H.R. Glyse in Rare Gas Solids Vol. II, ed. by M.L. Klein and J.A. Venables (Academic Press New York 1977).

(20) L. Schwalbe. Phys. Rev. B14, 1722 (1976).

(21) A.T. Macrander and R.K. Crawford. Phys. Stat. Sol. (a) 43, 611 (1977).

(22) W.G. Hoover and M. Ross. Contemp. Phys. 12, 339 (1971).

(23) W.B. Street, H.G. Raveché and R.D. Mountain. J. Chem. Phys. 61, 1960 (1974); R.D. Mountain and W.B. Street, ibid 61, 1970 (1974).

(24) J.P. Hansen and L. Verlet, Phys. Rev. 184, 151 (1969).

(25) F.H. Stillinger. J. Chem. Phys. 65, 3968 (1976).

(26) F.H. Stillinger and T.A. Weber. J. Chem. Phys. 68, 3837 (1978).

(27) See Ref. 12.

(28) P. Loubeyre, J.M. Besson, J.P. Pinceaux and J.P. Hansen. Phys. Rev. Lett. 49, 1172 (1982).

(29) D. Levesque, J.J. Weis and M.L. Klein. Phys. Rev. Lett. 51, 670 (1983).

(30) H.R. Glyde and M.G. Smoes. Phys. Rev. B22, 6391 (1980).

CHAPTER 6

DISCUSSION AND CONCLUSION

The objective in doing this work was to study the stability of crystals against large vibrational amplitudes and in a model including vacancies. The results presented here show that the lattice instability temperature (density) predicted by the SCP theory depends very sensitively on the approximation made to it. Firstly we discuss the effect of the approximations, and secondly we discuss the effect of including vacancies in the dynamics. The SCH and SCE approximations predict instability temperatures 10-300 times the observed melting temperatures T_M depending on the interatomic potentials. Generally, the steeper the hard core of the potential, the higher the instability temperatures predicted by the SCH and SCE models. When the cubic anharmonic term in the second order theory is added, the instability temperature of the RGC's is reduced to 1.5-5 times the melting temperatures. When the cubic term is added to the SCH model, specific phonon modes have imaginary (overdamped) frequencies at T_I. Once a branch becomes unstable, it is unstable over a wide range of q from low q up to $1/5^{th}$ of the Brillouin zone edge. It is possible to make an Einstein approximation to the SCH and SCH + C. The SCE and SCH approximations have similar stability. When the Einstein approximation was made to the SCH + C it was necessary to multiply the cubic shift by 2.36 in order to have the same instability temperature in the SCEC model as in SCH + C for the least stable phonons in Ar. The SCH + C which gives instability temperatures 3-5 times T_M gives a good description of the dynamics of RGC's up to and near T_M.[1] However, the full SCH + C calculation is complicated and requires long computing

times, so the simple Einstein model has advantages in studying the instabilities of crystals. In the stability study with dynamics and vacancies the simple Einstein approximation to SCH + C was used.

The central result of the work including vacancies is that the instability temperatures (densities) of the crystals can be predicted within 7-20% of the "observed" values. The "observed" values used for comparison are the maximum temperature (or minimum density) to which a crystal can be superheated in simulation studies of melting. It has been shown that in a system where there is a significant concentration of vacancies at high temperatures, such as in RGC's, a model including vacancies is important in determining crystal stability. We saw that in the SCEC model without vacancies, where the volume was held fixed at the observed value at melting for Ar the instability temperature is 4.6 times T_M. In the model where the volume is determined from the ISCE, instability temperature for Ar without vacancies is 145 K as opposed to 115 K for SCEC + vacancies. Street, Raveché and Mountain[2] in their Monte Carlo simulations of the Lennard-Jones system observed formation of vacancy-interstitial pairs near the instability point. Thus where vacancies play a role, they should be incorporated in any model studying lattice instability. In the Gaussian core model the vacancy concentration was found to be negligible, however, the instability temperatures were found to be in reasonable agreement with simulation values. It is interesting that only the dynamics is responsible for the good agreement with simulation in the GCM. The SCEC model with vacancies gives instability temperatures 1.4-1.6 times the melting temperatures for the RGC's depending on applied pressure.

The SCEC model while simple contains several approximations. The approximation made to the cubic term gives a shift that is too small because we have replaced all $\omega_{q\lambda}$, some of which are small transverse frequencies by a single large ω_E and $\bar{\Delta}(\omega_E)$ is inversely proportional to ω_E^4.

This is compensated for by multiplying the shift by 2.36 to give the same instability temperature for Ar as the SCH + C model. The same factor 2.36 was used in the cubic term of the ISCE free energy. It is interesting that the ISCE gives a reasonable enough equation of states for the RGC's. The ISCE also predicts thermodynamic properties similar to those of the self consistent averaged phonon theory of Paskin et al.[3] We observe that the lattice spacing a(T,P) predicted by the ISCE is 1-2% lower than the observed values at a given temperature. The smaller volume is responsible for predicting crystals that are more stable than would be observed. If the model predicted the correct volume it is conceivable that the SCEC model with vacancies might yield instability temperatures within a few percent of the observed melting temperatures. The error in the predicted lattice spacing increases with increasing applied pressures. Zubov[4] has found instability temperatures 1.3 to 1.5 times T_M for the RGC's, when including anharmonic terms to sixth order. This shows that vacancies do in fact play a key role in the instability of crystals.

The vacancy model we adopted is also very approximate. In this model only pair forces have been included. Also relaxations around vacancies have been neglected. Both of these approximations predict a larger vacancy formation enthalpy thus resulting in fewer vacancies. We have simply used a formation entropy $S = 2K_B$ consistent with experiment and other calculations for RGC's.[5] We believe that a more accurate model for vacancies would lead to lower enthalpy of formation thus giving

more vacancies. This would no doubt lower T_I bringing it closer to the observed T_M.

The GCM instability curve (fig. 10) is reminiscent of a similar curve for the bcc Wigner electron solid, showsn in fig. 15, calculated by Glyde and Keech[6] using the full SCH + C model; with the cubic term included in the iteration scheme in a manner similar to SCEC model. Their calculation included no vacancies. The shape of the two curves is similar and pressure melting takes place at small interparticle spacings in each case. In the quantum limit, the Wigner solid melts under pressure when the RMS vibrational amplitudes are large. This is not so in the GCM. We see in figs. 10 and 15 that SCEC instability curve and SCC instability line lie very much above the molecular dynamics points and the Monte Carlo line. In both cases the discrepancy increases with temperature. In the GCM we note that vacancies play no role at all, but in the Wigner solid vacancies might play a role. The SCC + vacancies model might therefore predict a lower instability temperature than the SCC model alone. We also see from table 11 that the Lindemann melting rule does not hold in the quantum limit. We see that in this limit δ can take any value $0.04 \leq \delta \leq 0.35$. However the rule is found to hold for thermal melting with the most accurate calculations giving $\delta \simeq 0.16$. Finally we note that when higher order terms in the SCP theory are included in the dynamics and thermal defects are taken into consideration, the predicted instability temperatures move closer to the observed values. Perhaps using the complete SCP theory which as is known predicts correct lattice spacing with vacancies would bring the predicted instability temperatures close to the observed melting temperatures. We conclude that the higher order SCP theory together

with the model containing vacancies contains some of the necessary ingredients for predicting reasonable instability parameters in real crystals.

REFERENCES

(1) M.L. Klein and T.R. Koehler, in Rare Gas Crystals ed. by M.L. Klein and J.A. Venables (Academic, New York 1976).

(2) W.B. Street, H.J. Raveché and R.D. Mountain. J. Chem. Phys. 61, 1960 and 1970 (1974).

(3) K. Shukla, A. Paskin, D.O. Welch and G.J. Dienes. Phys. Rev. B24, 724 (1981).
A. Paskin, A.M. Llois de Kreiner, K. Shukla, D.O. Welch and G.J. Dienes, ibid 25, 1297 (1982).

(4) V.I. Zubov. Phys. Stat. Sol. (b), 87, 385 (1978), 88, 43 (1978).

(5) A.V. Chadwick and H.R. Glyde in Rare Gas Crystals, Vol. II, ed. by M.L. Klein and J.A. Venables (Academic New York 1976).

(6) H.R. Glyde and G.H. Keech. Ann. Phys. (New York), 127, 330 (1980).

(7) W.L. Slatterly, G.D. Doolen and H.E. DeWitt. Phys. Rev. A26, 2255 (1982), A21, 2087 (1980).

(8) D. Ceperley, in Recent Progress in Many-Body Theories, Lecture Notes in Physics No. 142 ed. by J.G. Zabolitsky, M. de Llamo, M. Forbes and J.W. Clarke (Springer-Verlag New York 1981), pg. 262.

TABLE CAPTIONS

Table 1: The Morse potential parameters eqn. (4.4), reference 13, chapter 4.

Table 2: Instability temperatures of rare gas crystals in different approximations of the self consistent phonon theory. T_M is the observed melting temperature.

Table 3: Lindemann ratios for rare gas crystals for SCE, SCH and SCEC approximations to SCP at T_I.

Table 4: Morse potential parameters $R_o(A^o)$, D(K) for Ar for arbitrary values of γ.

Table 5: Comparison of instability temperature for Ar with SCE and SCH models at different values of γ.

Table 6: Zero pressure instability temperatures, reduced vibrational amplitudes and vacancy concentration in rare gas crystals.

Table 7: Vacancy concentration C and formation enthalpy at the observed T_M, calculated in SCEC + V model.

Table 8: The instability densities ρ_I in the Monte Carlo simulations and in the SCEC + V model for Lennard-Jones Argone (ϵ = 119.86 K, σ = 3.405 A^o).

Table 9: Reduced instability temperatures T_I^* for selected reduced densities in the Gaussian core model with SCE, SCEC and molecular dynamics T_I^* and T_M^*, reference 25-27, chapter 5.

Table 10: Reduced instability pressure (P_I^*), temperature (T_I^*) and vacancy concentration (C_I^*) versus reduced density (ρ^*).

Table 11: Instability density and Lindemann ratio δ in the bcc and fcc Gaussian core model in thq quantum limit (0 K). The choice of ϕ_o and ℓ simulate Ar (M = 40) and Ne (M = 20 and M = 5). Also listed are the quantum melting values of δ in solid helium and the Wigner electron solid. All masses M in amu.

TABLE 1. Morse potential parameters equn. (4.4)

	γ A^{o-1}	D K	R_o A^o
Xe	1.35	287.3	4.3937
Kr	1.52	207.5	4.0216
Ar	1.55	146.8	3.7682
Ne	1.85	44.6	3.0446

TABLE 2. Instability temperatures for rare gas crystals in different approximations of the SCP theory T_M(K) is the observed melting temperature, T_I(K) is the instability temperature.

	SCE	SCH	SCH + C	SCE + C	SCEC	T_M
Ne	32,000			80	72	25
Ar	15,180	20,500	380	395	380	83
Kr	32,000		450	465	450	116
Xe	34,000	54,000	750	780	760	161

TABLE 3. Lindemann ratios for rare gas crystals for SCE, SCH and SCEC approximations to the SCP theory at T_I.

Element	δ SCE	SCH	SCEC
Ne	0.30		
Ar	0.29	0.31	0.160
Kr	0.29		0.163
Xe	0.30	0.32	0.160

TABLE 4. Morse potential parameters $R_o(A^o)$, D(K) for Ar for arbitrary values of γ.

$\gamma(A^{o-1})$	D(K)	$R_o(A^o)$
1.1	109.966	3.890
1.55	146.80	3.768
1.65	154.71	3.742
1.75	160.21	3.732
1.85	164.71	3.723
1.95	168.85	3.720
2.05	172.55	3.715

TABLE 5. Comparison of instability temperature for Ar with SCE and SCH models at different values of γ.

$\gamma(A^{o-1})$	$T_{I(K)}$ SCE	SCH
1.1	2250	7000
1.55	15180	20500
1.66	21900	
1.75	25820	
1.85	25820	
1.95	25802	25000
2.05	25820	

TABLE 6. Zero pressure instability temperatures, reduced vibrational amplitudes and vacancy concentration in the RGC's.

Element	T_M(K)	T_I(K)	δ_I	C_I
Ar	83	115	0.163	2.9×10^{-2}
Kr	115	155	0.160	2.4×10^{-2}
Xe	160	225	0.162	3.5×10^{-2}

TABLE 7. Vacancy concentration C and formation enthalpy at the observed T_M calculated in SCEC + V model.

Element	T_M(K)	h(T)(K)		$C(T_M)$	
	obs	calc	obs	calc	
Ar	83	—	857	$<2 \times 10^{-4}$(a) $<3 \times 10^{-3}$(b)	3.5×10^{-4}
Kr	115	890(±100)[c]	1192	3.2×10^{-3}[c]	5.6×10^{-4}
Xe	160	$1100(^{+400}_{-150})$[d]	1690	8.2×10^{-3}[d]	4.6×10^{-4}

(a) Schwalbe, Ref. 20, chapter 5.

(b) Macrander and Crawford, Ref. 21, chapter 5.

(c) Losee and Simmons, Ref. 3, chapter 5.

(d) Granfors et al, Ref. 18, chapter 5.

TABLE 8. The instability densities ρ_I found in MC simulations and in the present SCEC + V model for Lenhard-Jones Ar(ε = 119.86 K, σ = 3.405 A°) $\rho = (\sigma^3 N/V)$.

$T^* = \frac{K_B T}{\varepsilon}$	T(K)	ρ_M	ρ_M(MC)	ρ_I (SCEC)	$\frac{\rho_M}{\rho_I}$ (MC)	$\frac{\rho_M}{\rho_I}$ (SCEC)
1.06	127	1.012[c]	0.899[a]	0.868	1.126	1.16
1.17	140	1.024[c]	0.933[b]	0.875	1.097	1.17
2.74	327	1.179[c]	1.097[b]	0.940	1.075	1.25
2.74	327	1.179[c]	1.058[a]	0.940	1.114	—
Hard spheres[a]		1.041	0.943	—	1.104	—

(a) Hoover and Ross, Ref. 22, chapter 5.

(b) Street and co-workers, Ref. 23, chapter 5.

(c) Hansen and Verlet, Ref. 24, chapter 5.

TABLE 9. Reduced instability temperatures T_I^* for selected reduced densities ρ^* with SCE, SCEC, and MD T_I^* and MD T_M^* (Gaussian core model).

ρ^*	SCE	SCEC	MD $T_I^{*(a)}$	MD $T_M^{*(a)}$
0.2	84.5×10^{-3}	12.63×10^{-3}	10.3×10^{-3}	8.12×10^{-3}
0.4	92.5×10^{-3}	13.12×10^{-3}	8×10^{-3}	6.2×10^{-3}
1.0	89.12×10^{-3}	7.63×10^{-3}	7.8×10^{-4}	6.0×10^{-4}

(a) Stillinger and Weber, Ref. 25-27, chapter 5.

TABLE 10. Reduced instability pressure (P_I^*), temperature (T_I^*) and vacancy concentration (C_I^*) versus reduced density (ρ^*).

ρ^*	P_I^*	T_I^*	C_I
0.3	0.206	1.40×10^{-2}	6.1×10^{-7}
0.4	0.45	1.312×10^{-2}	5.7×10^{-13}
0.8	1.82	8.87×10^{-3}	2.75×10^{-24}
1.0	2.82	7.625×10^{-3}	6.03×10^{-28}

TABLE 11. Instability density and Lindemann ratio δ in the bcc and fcc GCM crystals in the quantum limit (0 K). The choice of ϕ_o and ℓ simulate Ar (M = 40) and Ne (M = 20 and M = 5). Also listed are the quantum melting values of δ in solid helium and the Wigner electron solid.

M (amu)	ϕ_o 10^5 K	ℓ A°	ρ^* (fcc)	δ	ρ^* (bcc)	δ
40	8.49	1.192	6.1	0.040	2.9	0.048
20	2.59	0.964	3.5	0.086	1.7	0.081
5	2.59	0.964	1.7	0.091	0.8	0.094

Solid helium (bcc) $\delta = 0.35$

Wigner solid (bcc) $\delta = 0.26$

FIGURE CAPTIONS

Fig. 1 Zero pressure lattice constant dilation with temperature in Ar, Kr and Xe. The ISCE is the present improved self consistent Einstein model with the Lennard-Jones, Morse and Aziz Chen (Ref. 9, chapter 4) potentials. The ISC (B.B.) is the ISC theory calculated using Bobetic-Barker (Ref. 4, chapter 4). The observed dilations are from references 16, 17 and 18, chapter 4.

Fig. 2 Zero pressure isothermal bulk modulus with same key as fig. 1. The ISC (BFW) 3-body uses the Barker-Fisher-Watts (Ref. 5, chapter 4) potential plus three body Axilrod-Teller forces. The observed values are from Anderson and Swenson (Ref. 19), Peterson et al (Ref. 16), Urvas et al (Ref. 20), Korpiun and Coufal (Ref. 21) and Korpiun et al (Ref. 22). All references in chapter 4.

Fig. 3 The ratio of the square of the self consistent Einstein frequency to the static crystal Einstein frequency as a function of δ.

Fig. 4 The SCE free energy equation (2.31) (multiplied by 10^4) as a function of δ at different temperatures in Ar. The T_I in the SCE model is 15,180 K.

Fig. 5 The temperature dependence of the SCH + cubic phonon frequencies along the T_1 [q, q, 0] branch, for the reduced wavevector q values shown, in Ar fixed at the volume shown.

Fig. 6 The variation of the SCEC frequency with $\delta = (\langle u^2 \rangle / R^2)^{1/2}$

Fig. 7 The variation of square of the SCEC + vacancies with temperature.

Fig. 8 The SCEC + vacancies instability curves compared with the observed melting curves. The observed values are from Daniels and his co-workers (Ref. 13, 14) for Ar and Kr and Stryland et al (Ref. 15) in Xe. All references in chapter 5.

Fig. 9 The SCEC + V vacancy concentration versus the inverse temperature. The observed values are from Schwalbe (Ref. 20), Losee and Simmons (Ref. 17) and Granfors et al (Ref. 18). The Monte Carlo calculations are from Squire and Hoover (Ref. 16). All references in chapter 5.

Fig. 10 The SCEC + V bcc crystal instability curve for the Gaussian core model, compared with molecular dynamics T_I and T_M of Stillinger and Weber (Ref. 26, 27) QL marks SCEC + V instability volume in the quantum limit (T = 0 K) calculated with the Gaussian core potential set to simulate Ar (M = 40 amu) H is the instability volume in the Einstein approximation. References in chapter 5.

Fig. 11 The Lindemann ratio δ versus temperature in the Gaussian core model for $\rho^* = 0.2$. The open circles are from Stillinger and Weber (Ref. 27) the continuous line is the present SCEC + V model. References from chapter 5.

Fig. 12. The square of SCEC + V frequency versus reduced temperature for the GCM at $\rho^* = 0.2$.

Fig. 13 The Gaussian core model potential.

Fig. 14 The SCH dispersion curves for the GCM compared and Aziz-Chen potentials for Ar (M = 40) at $\rho^* = 0.2$.

Fig. 15 The instability curve of the Wigner electron crystal calculated in the self consistent phonon theory (SCC) compared with the Monte Carlo (MC) melting lines. MC melting is the classical melting line of Slatterly and his co-workers (Ref. 7) given by $K_R T_M = 2/(\Gamma_M r_s)$ with $\Gamma_M = 178$. The arrow (MC is the T = 0) pressure melting r_s value ($r_s = 165$), calculated by Ceperley (Ref. 8) for the charged Bose system ($\vec{r} = r_s a_o$, $a_o = 0.529172$ Å). K_R is the Boltzmann's constant in Rydberg units (1 Ryd = $e^2/2a_o$ = 13.6048 eV). To the left of the dashed line quantum effects are important.

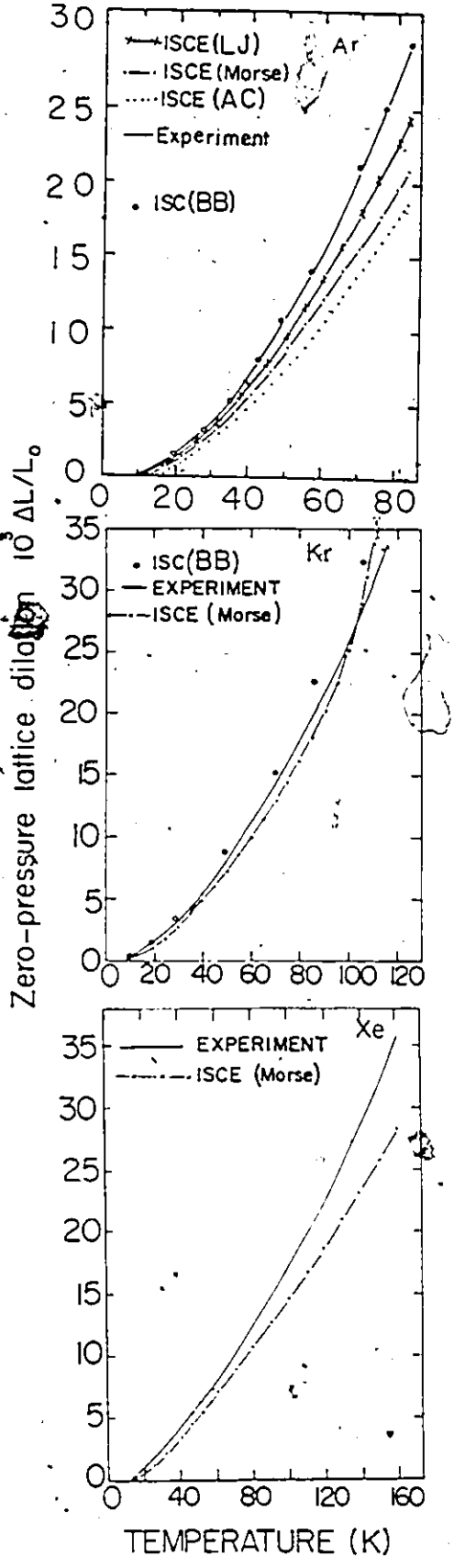
ISCE(LJ)
ISCE (Morse)
ISCE (AC)
Experiment
ISC(BB)
Ar
Kr
EXPERIMENT
Xe
Zero-pressure lattice dilation $10^3 \Delta L/L_o$
TEMPERATURE (K)

FIG 1

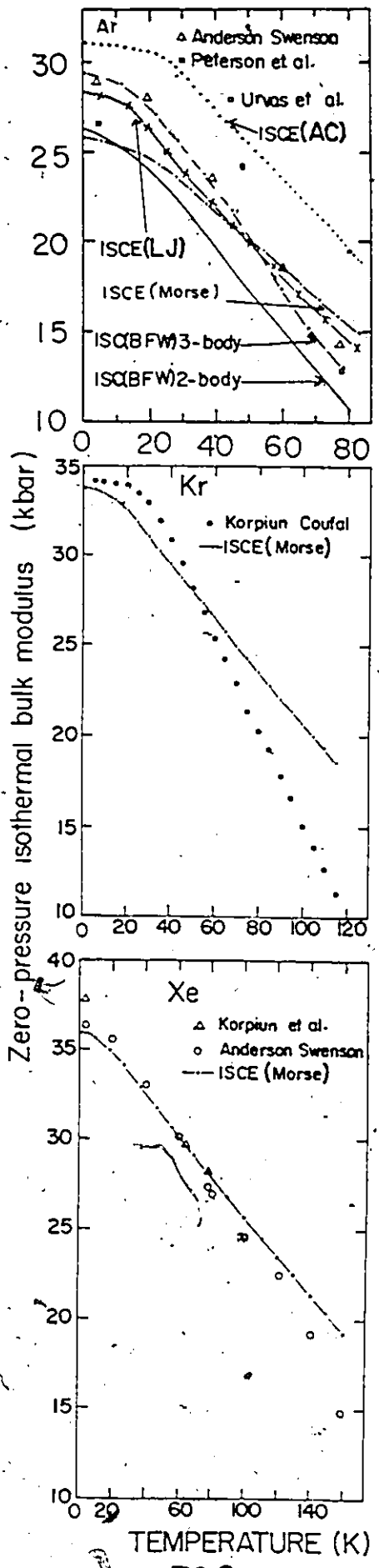
Ar
Anderson Swenson
Peterson et al.
Urvas et al.
ISCE(AC)
ISCE(LJ)
ISCE(Morse)
ISCE(BFW)3-body
ISCE(BFW)2-body
Kr
Korpiun Coufal
ISCE(Morse)
Xe
Korpiun et al.
Anderson Swenson
ISCE (Morse)
Zero-pressure isothermal bulk modulus (kbar)
TEMPERATURE (K)

FIG·2

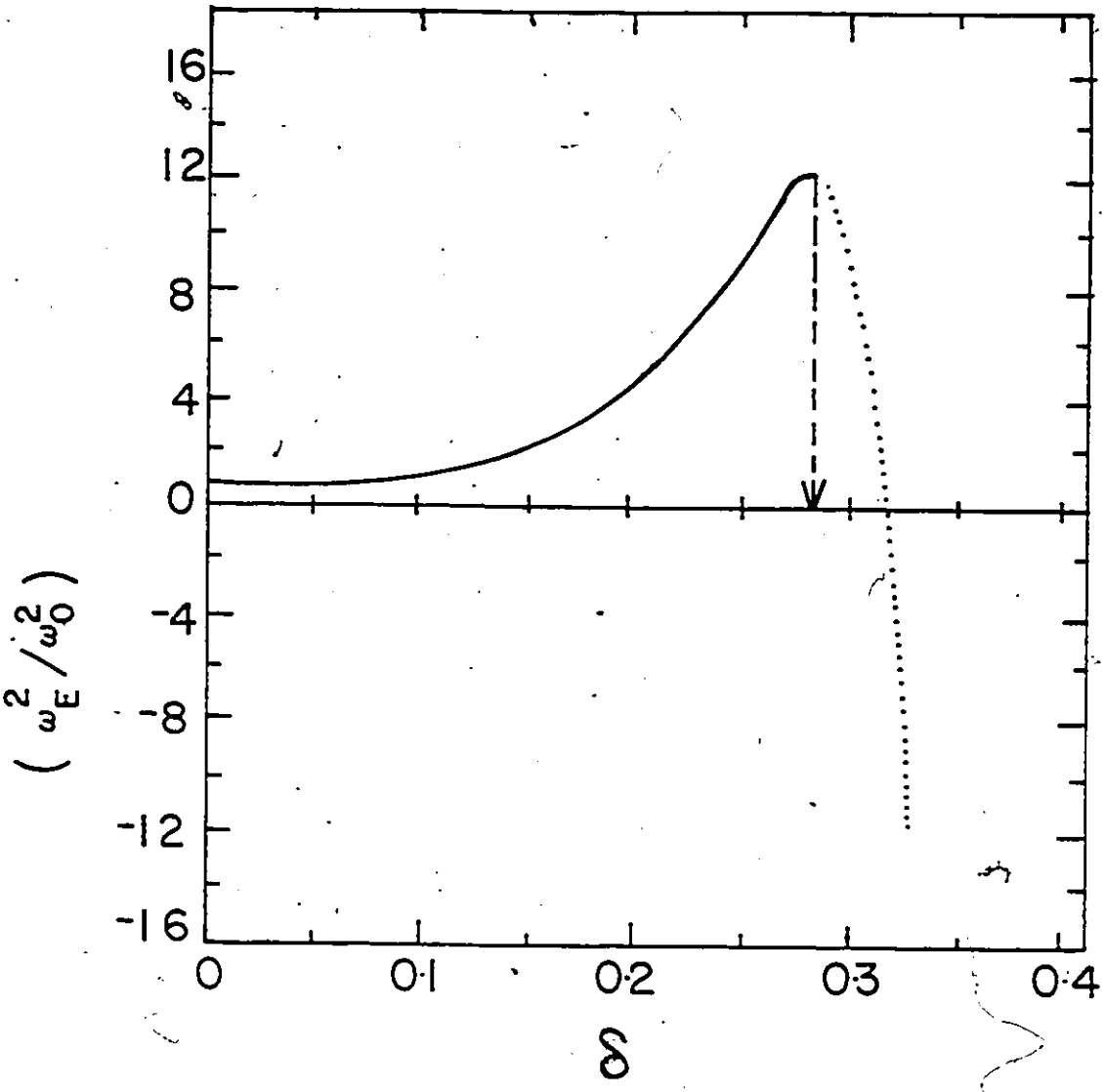

FIG·3

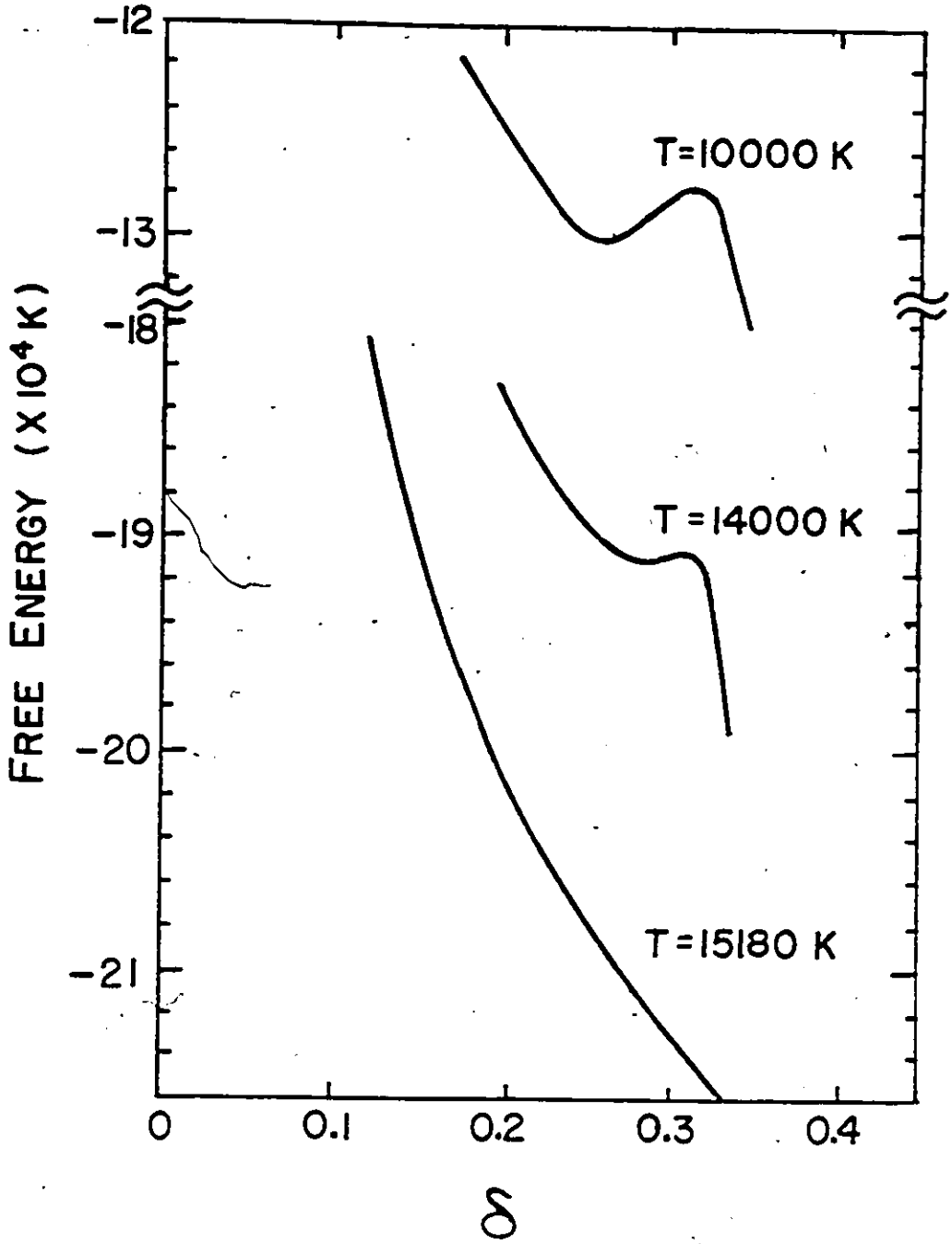
-12
-13
-18
-19
-20
-21
FREE ENERGY (X 10⁴ K)
T=10000 K
T = 14000 K
T=15180 K
0
0.1
0.2
0.3
0.4
δ

FIG. 4

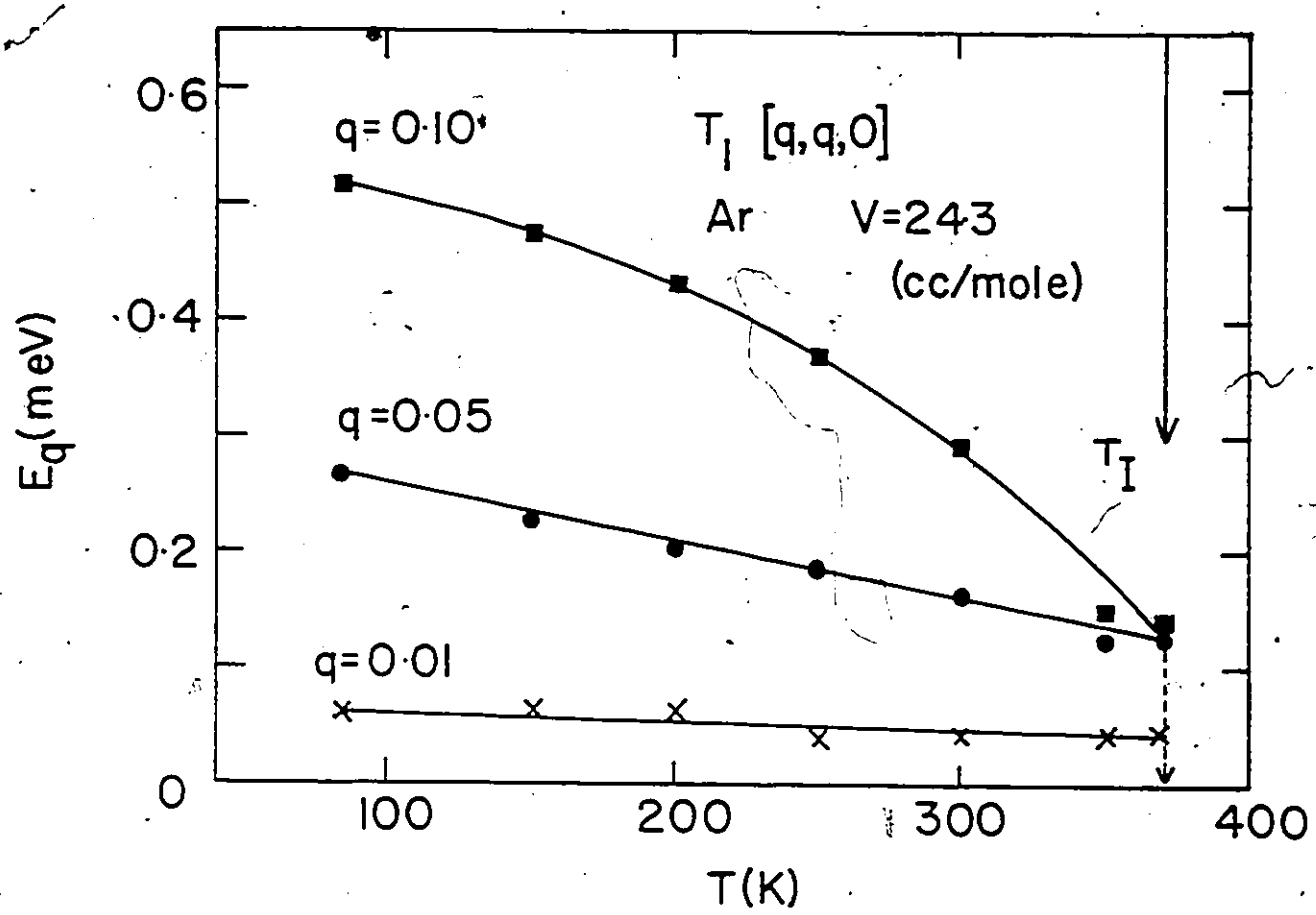
0·6
0·4
0·2
0
E_q(meV)
q=0·10
q=0·05
q=0·01
T_I [q,q,0]
Ar V=243
(cc/mole)
T_I
100
200
300
400
T(K)

FIG·5

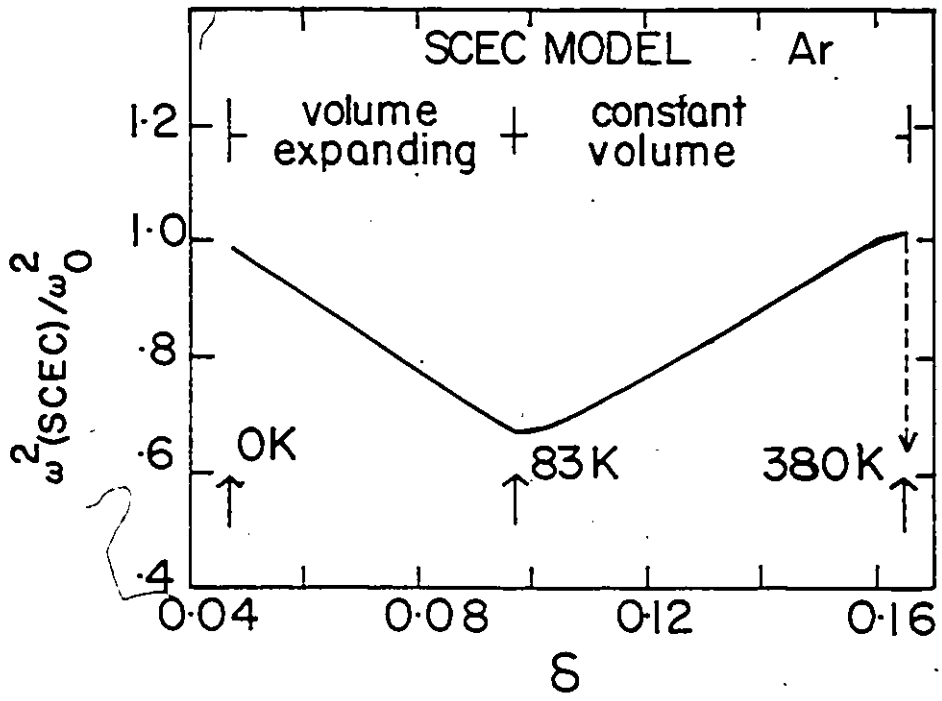
SCEC MODEL Ar
volume expanding
constant volume
1·2
1·0
·8
·6
·4
0K
83K
380K
0·04
0·08
0·12
0·16
δ
$\omega^2_{(SCEC)}/\omega^2_0$

FIG. 6

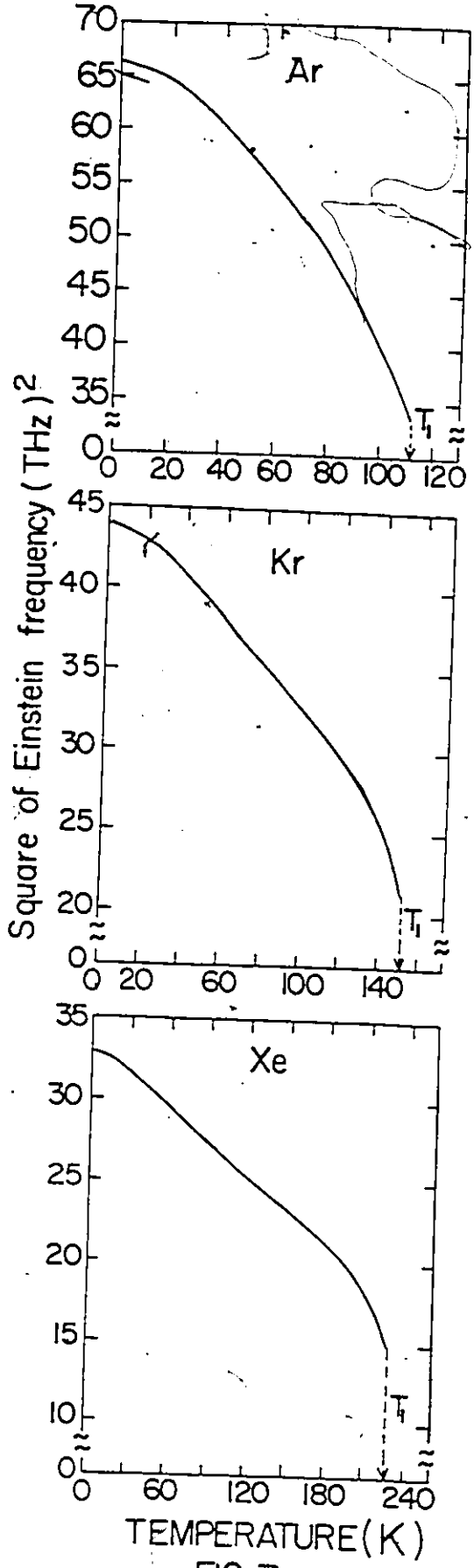
Ar
Kr
Xe
Square of Einstein frequency (THz)^2
TEMPERATURE(K)
T_1
T_1
T_1

FIG·7

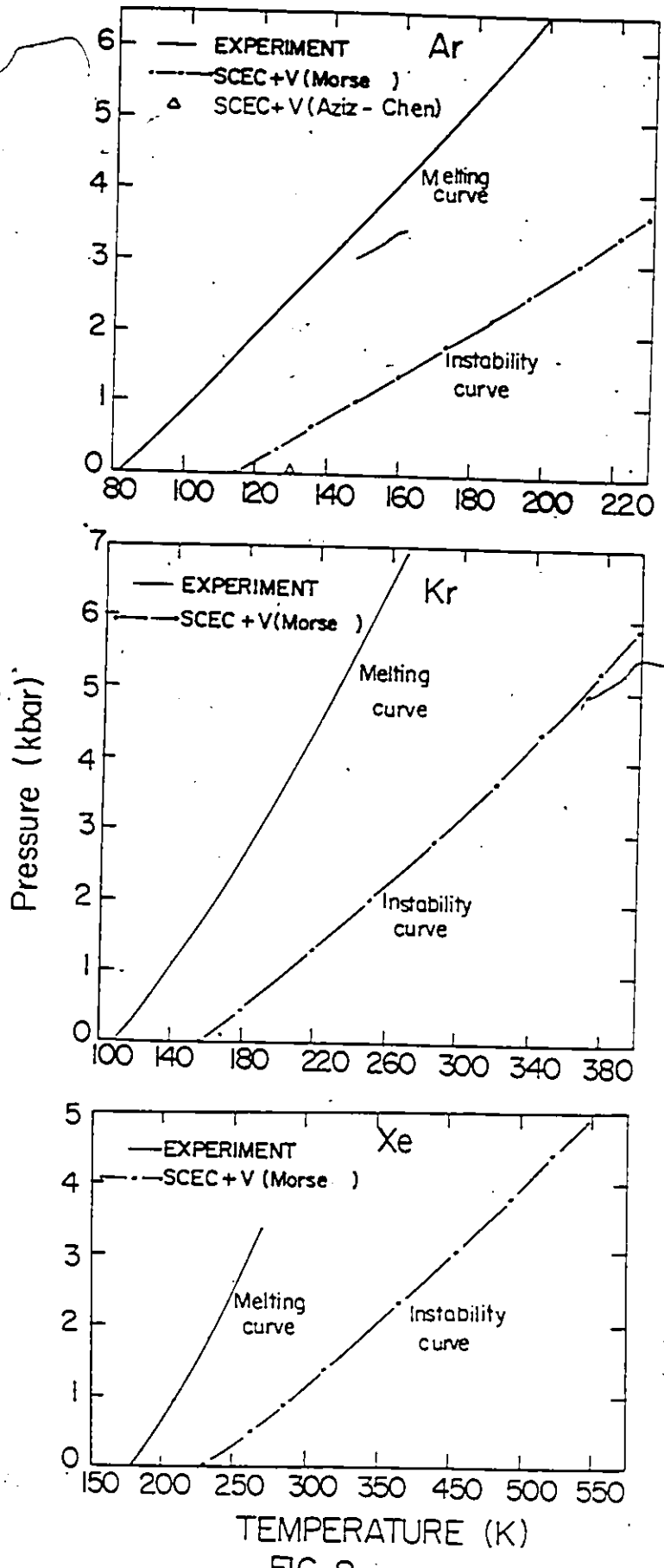
EXPERIMENT
SCEC+V (Morse)
SCEC+V (Aziz - Chen)
Ar
Melting curve
Instability curve
Kr
Xe
Pressure (kbar)
TEMPERATURE (K)

FIG. 8

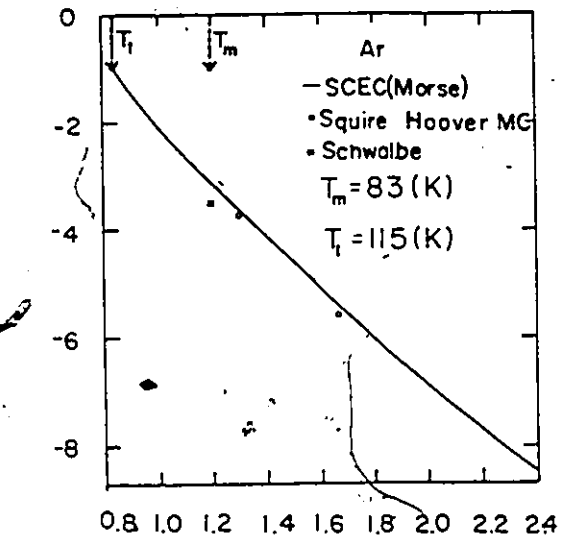
Ar
SCEC(Morse)
Squire Hoover MC
Schwalbe
T_m=83 (K)
T_t=115 (K)
T_t
T_m
0
-2
-4
-6
-8
0.8 1.0 1.2 1.4 1.6 1.8 2.0 2.2 2.4

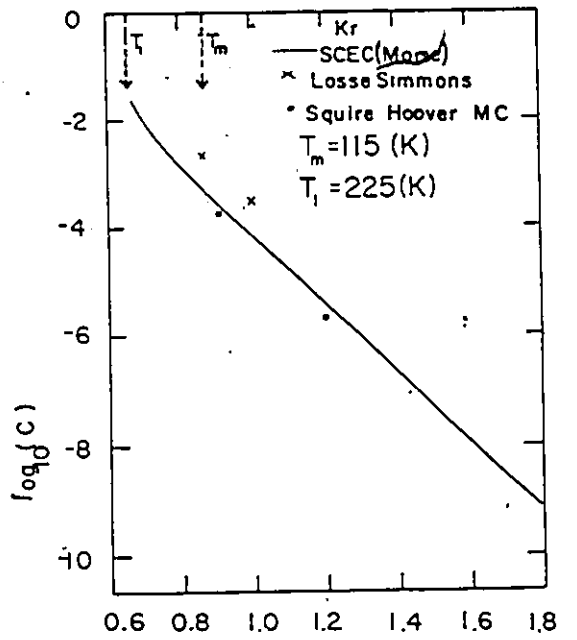
Kr
SCEC(Morse)
Losse Simmons
Squire Hoover MC
T_m=115 (K)
T_t=225(K)
T_t
T_m
$\log_{10}(C)$
0
-2
-4
-6
-8
-10
0.6 0.8 1.0 1.2 1.4 1.6 1.8

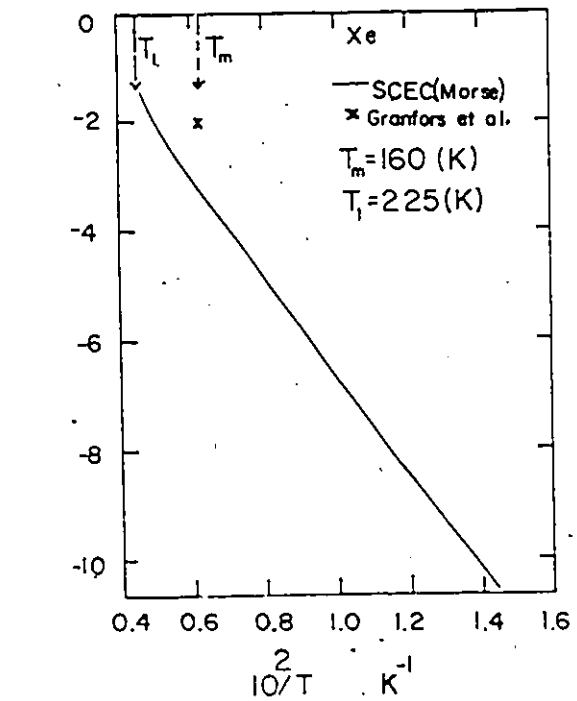
Xe
SCEC(Morse)
Granfors et al.
T_m=160 (K)
T_t=225(K)
T_t
T_m
0
-2
-4
-6
-8
-10
0.4 0.6 0.8 1.0 1.2 1.4 1.6
$10^2/T$ K^{-1}

FIG·9

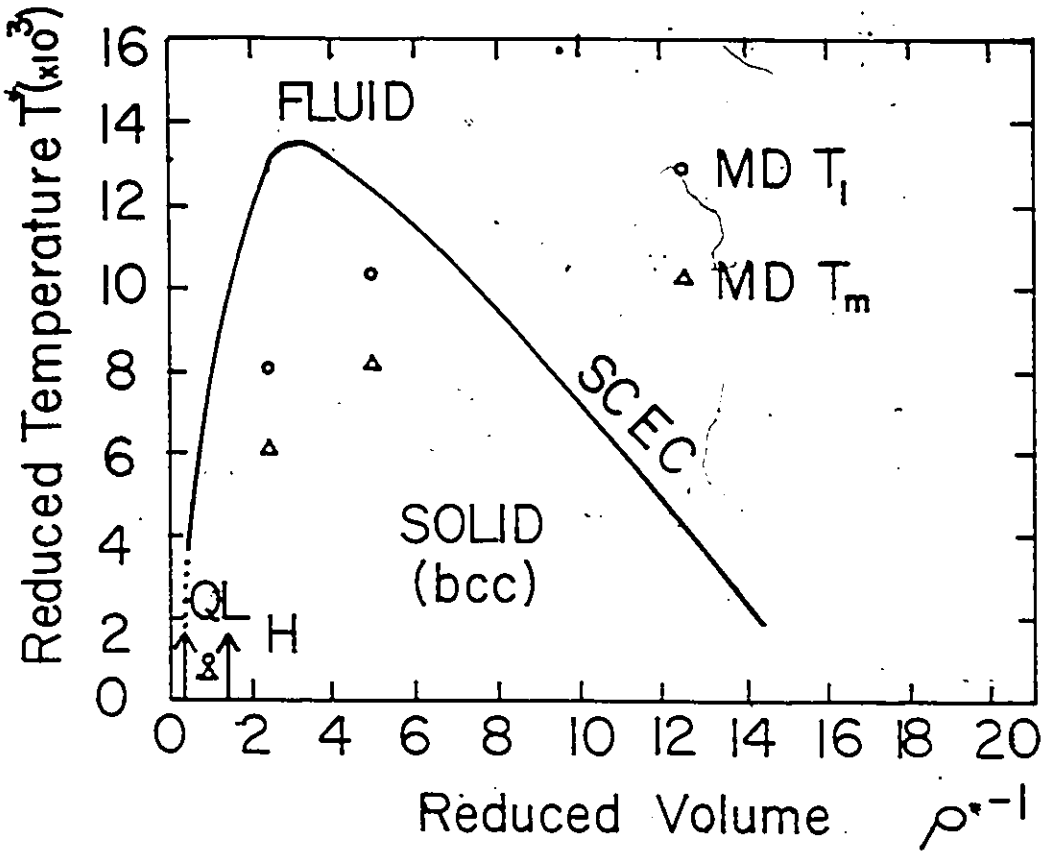
Reduced Temperature $T^*(\times 10^3)$
16
14
12
10
8
6
4
2
0
FLUID
MD T_l
MD T_m
SCEC
SOLID
(bcc)
QL
H
0
2
4
6
8
10
12
14
16
18
20
Reduced Volume ρ^{*-1}

FIG. 10

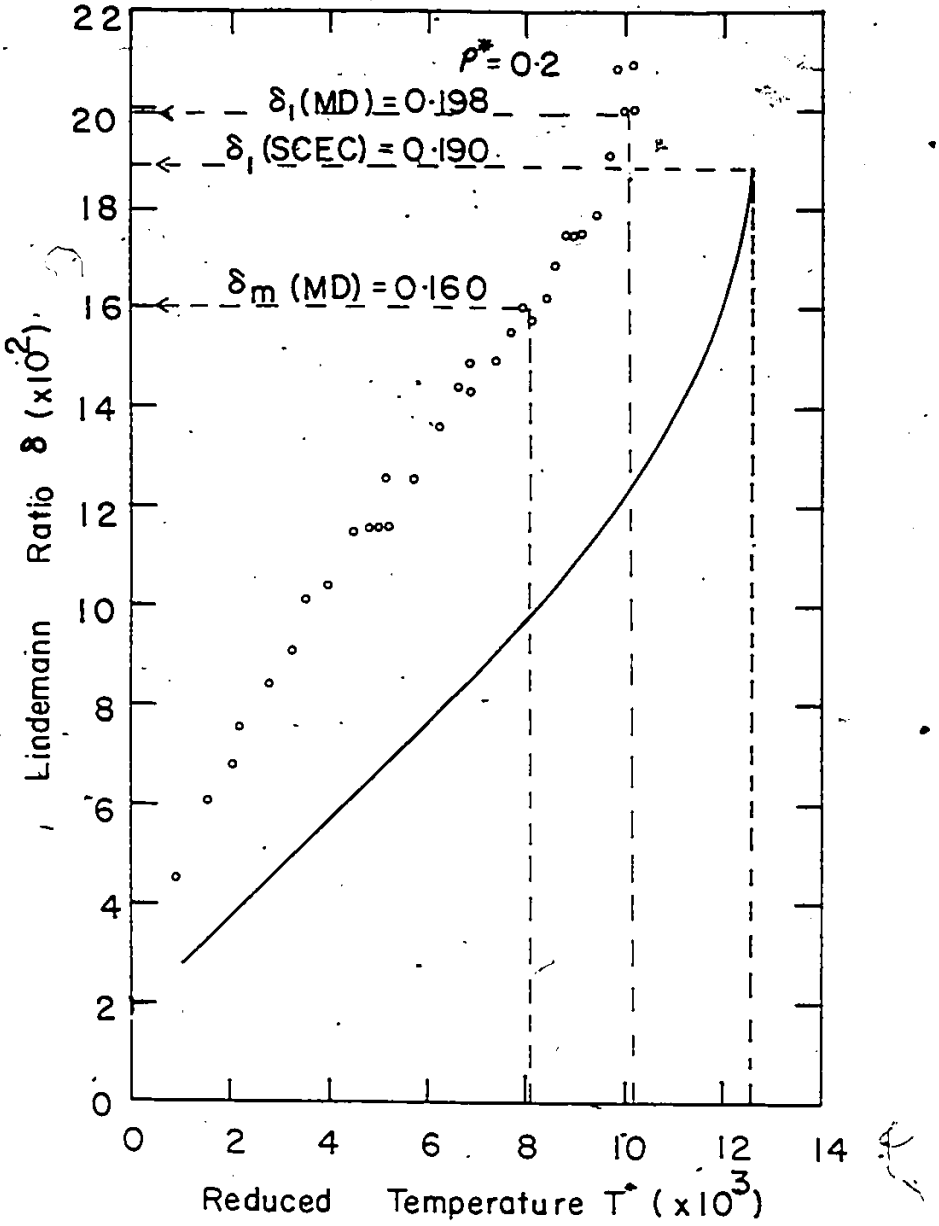
$\rho^* = 0.2$
δ_l (MD) = 0.198
δ_l (SCEC) = 0.190
δ_m (MD) = 0.160
Lindemann Ratio δ ($\times 10^{-2}$)
Reduced Temperature T^* ($\times 10^{-3}$)
0
2
4
6
8
10
12
14
16
18
20
22

FIG. 11

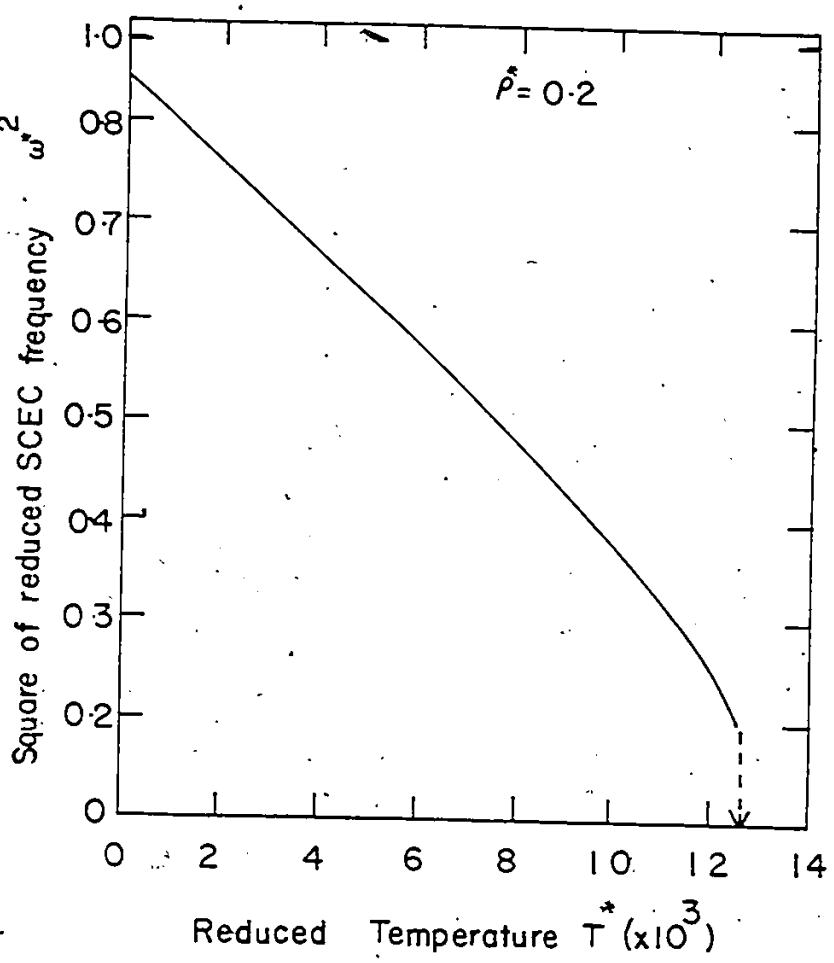
$\rho^* = 0.2$
Square of reduced SCEC frequency ω^{*2}
1·0
0·8
0·7
0·6
0·5
0·4
0·3
0·2
0
0 2 4 6 8 10 12 14
Reduced Temperature T^* ($\times 10^3$)

FIG. 12

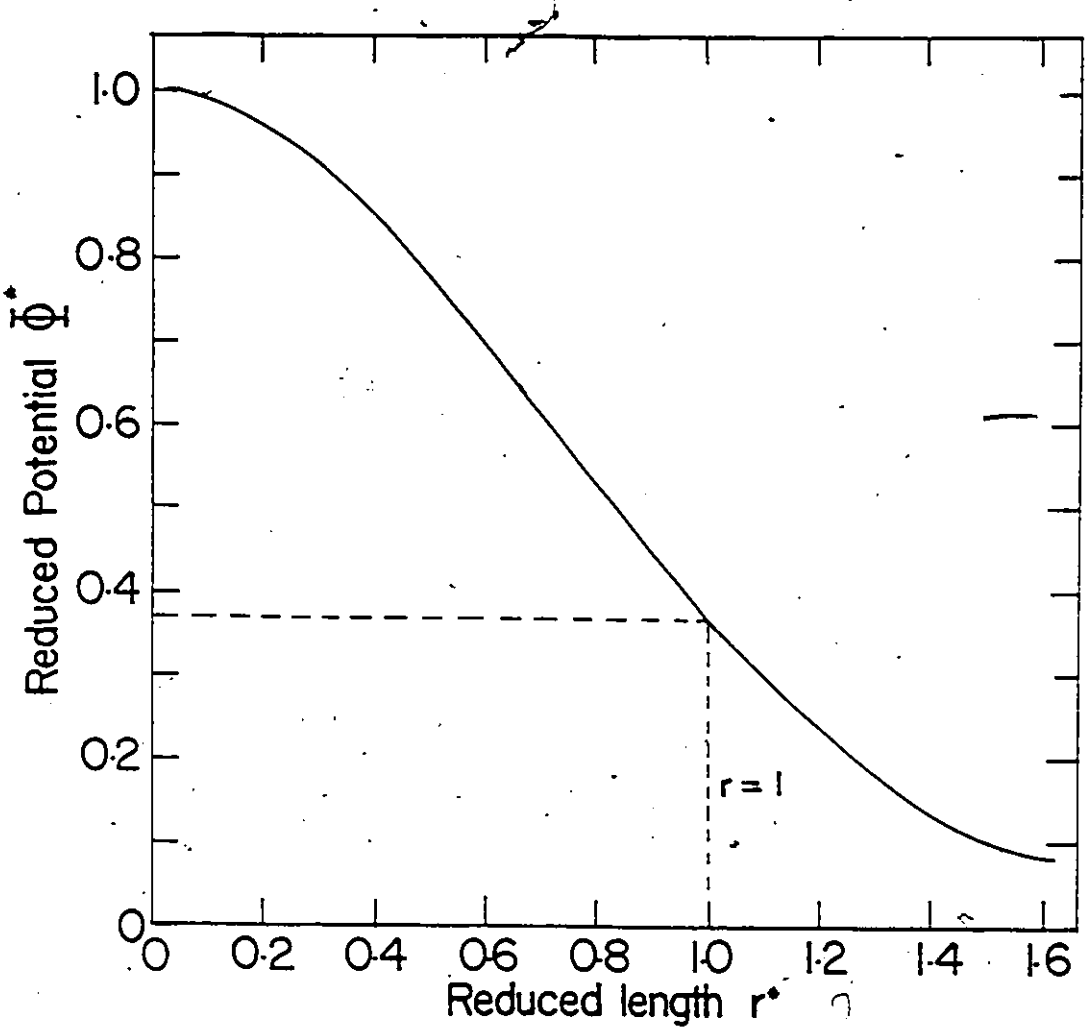
1·0
0·8
0·6
0·4
0·2
0
Reduced Potential Φ*
r = 1
0
0·2
0·4
0·6
0·8
1·0
1·2
1·4
1·6
Reduced length r*

FIG. 13

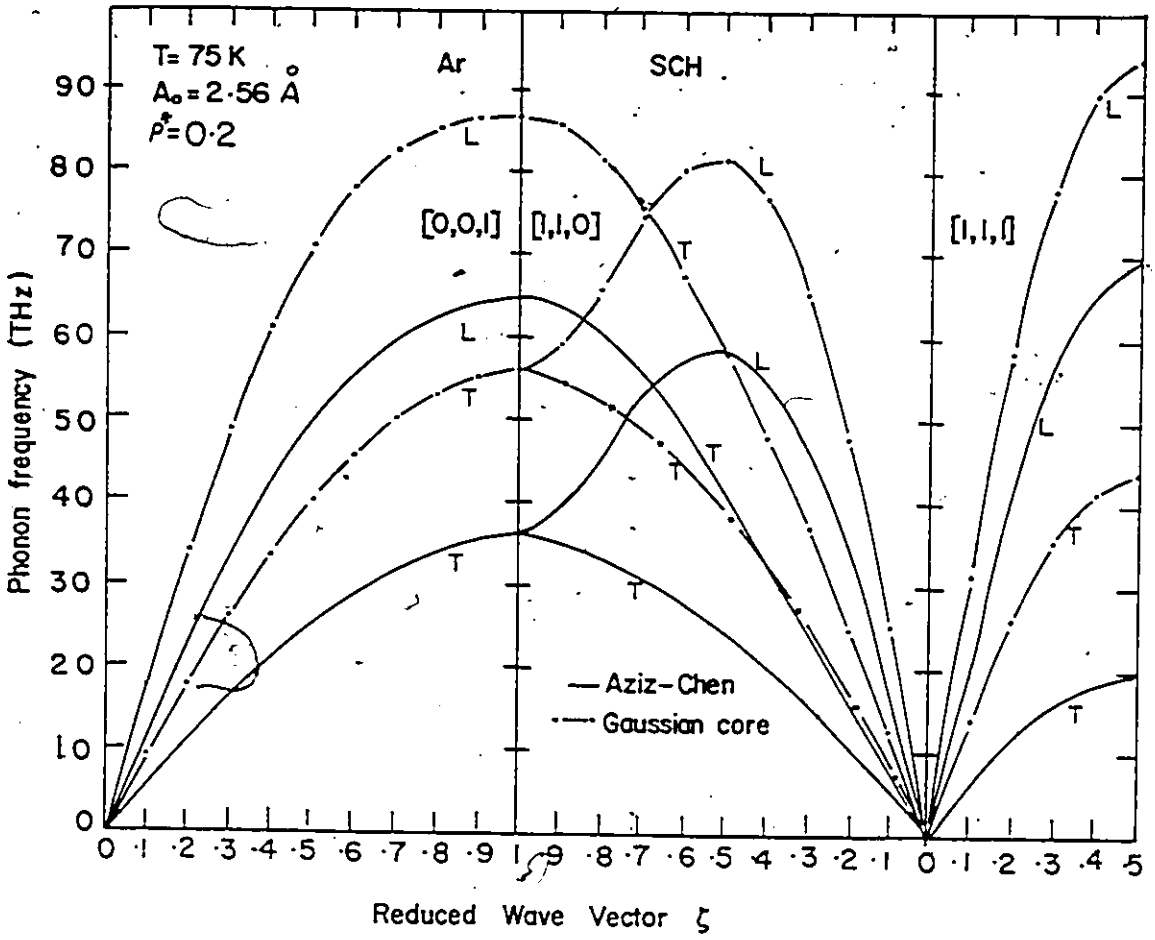
T= 75 K
A₀ = 2·56 Å
ρ* = 0·2
Ar
SCH
[0,0,1]
[1,1,0]
[1,1,1]
L
T
— Aziz-Chen
·— Gaussian core
Phonon frequency (THz)
Reduced Wave Vector ζ

FIG. 14

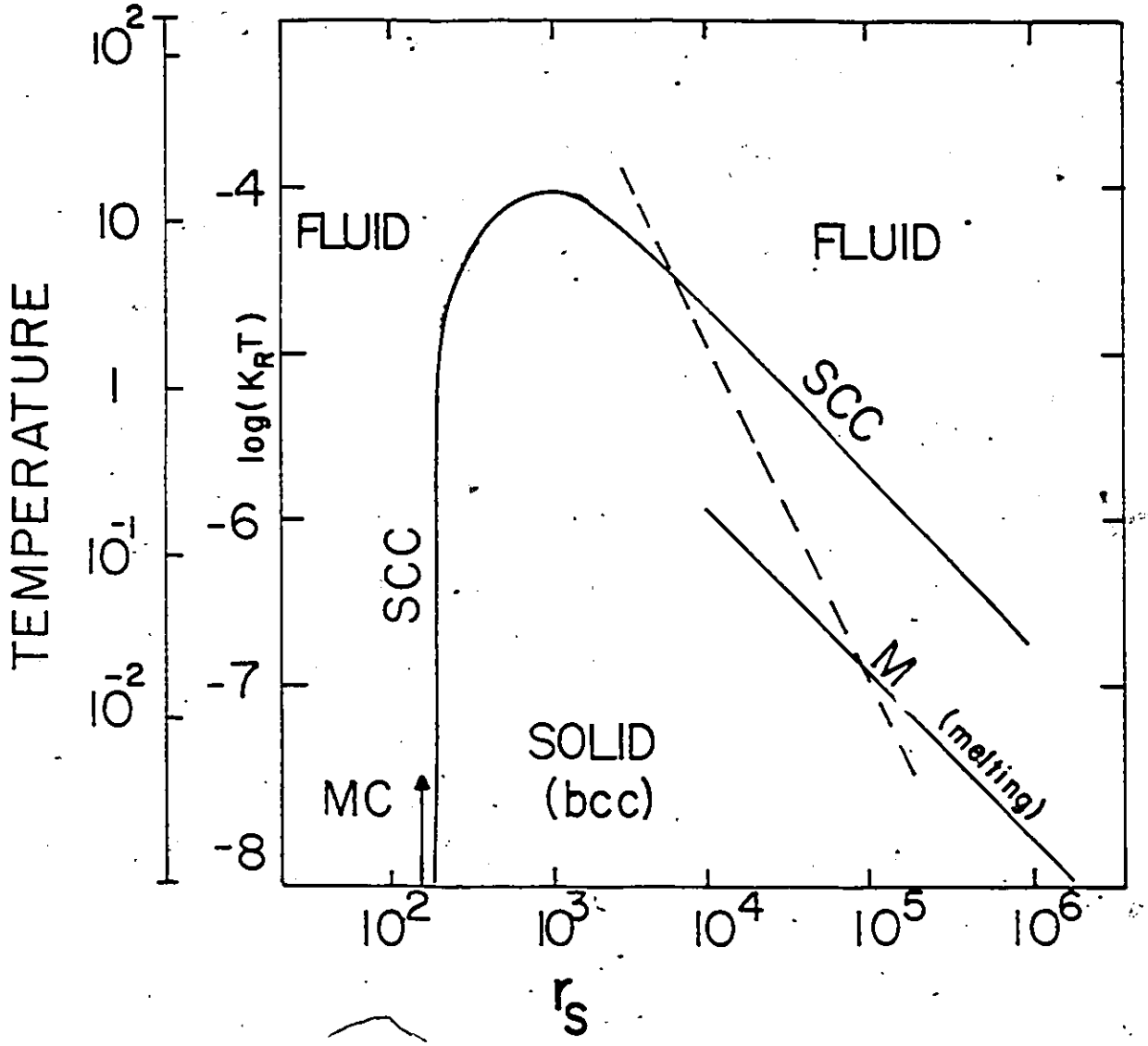
TEMPERATURE
10^2
10
1
10^{-1}
10^{-2}
-4
-6
-7
-8
log(K_BT)
FLUID
FLUID
SCC
SCC
M
(melting)
SOLID
(bcc)
MC
10^2
10^3
10^4
10^5
10^6
r_s

FIG. 15

APPENDIX

Cubic Einstein Approximation

The frequency of phonon having wave vector q and branch index λ including the cubic term as a perturbation (and assuming the frequency dependence of Δ and Γ in (2.11) is small) is

$$\omega^2(q\lambda) = \bar{\omega}^2_{q\lambda} + 2\omega_{q\lambda}\Delta(q\lambda,\omega). \tag{A1}$$

Here the cubic shift is

$$\Delta(1,\omega) = -\frac{1}{2\hbar^2} \sum_{\substack{q_2\lambda_2 \\ q_3\lambda_3}} |V(1,2,3)|^2 M(1,2,\omega)\Delta(\vec{q}_1+\vec{q}_2+\vec{q}_3) \tag{A2}$$

where

$$V(1,2,3) = \left(\frac{\hbar}{2NM}\right)^{3/2} \left(\frac{1}{\omega_1\omega_2\omega_3}\right)^{1/2} \sum_{\substack{\ell_1\ell_2\ell_3 \\ \alpha_1\alpha_2\alpha_3}} \phi_{\alpha_1\alpha_2\alpha_3}(\ell_1\ell_2\ell_3) \cdot$$
$$\times e^{i\vec{q}_1\cdot\vec{R}_1} e^{i\vec{q}_2\cdot\vec{R}_2} e^{i\vec{q}_3\cdot\vec{R}_3} \varepsilon_{\alpha_1}(1)\ \varepsilon_{\alpha_2}(2)\ \varepsilon_{\alpha_3}(3) \tag{A3}$$

$$M(2,3,\omega) = (n_2+n_3+1)\left[\frac{1}{\omega_2+\omega_3+\omega} + \frac{1}{\omega_2+\omega_3-\omega}\right]$$
$$+ (n_2-n_3)\left[\frac{1}{\omega_2-\omega_3+\omega} + \frac{1}{\omega_2-\omega_3-\omega}\right] \tag{A4}$$

and $1 = q_1\lambda_1$. The $\Delta(\vec{q}_1+\vec{q}_2+\vec{q}_3)$ means that q_3 is fixed by $\vec{q}_3 = -(\vec{q}_1+\vec{q}_2)$

in the sum over q_3.

We define the Einstein frequency, as in the harmonic case, as the mean square frequency,

$$\omega^2(\text{SCEC}) \equiv \frac{1}{3N} \sum_{q\lambda} \omega^2(q\lambda)$$

$$= \frac{1}{3N} \sum_{q\lambda} \omega_{q\lambda}^2 + \frac{1}{3N} \sum_{q\lambda} 2\omega_{q\lambda}\Delta(q\lambda,\omega). \tag{A5}$$

We also approximate ω and each $\omega_{q\lambda}$ in $\Delta(q\lambda,\omega)$ by the harmonic Einstein frequency (25), i.e.

$$\omega^2(\text{SCEC}) = \omega_E^2 + 2\omega_E \bar{\Delta}(\omega_E) \tag{A6}$$

where

$$\bar{\Delta}(\omega_E) \equiv \frac{1}{3N} \sum_{q\lambda} \Delta(q\lambda,\omega_E). \tag{A7}$$

With this approximation,

$$M(2,3,\omega_E) = [2n(\omega_E)+1] \frac{4}{3\omega_E} \tag{A8}$$

and

$$|V(1,2,3)|^2 = \left(\frac{\hbar}{2MN\omega_E}\right)^3 \left[\sum_{\substack{\ell_1\ell_2\ell_2 \\ \alpha_1\alpha_2\alpha_3}} \phi_{\alpha_1\alpha_2\alpha_3}(\ell_1\ell_2\ell_3) e^{-i(\vec{q}_1\cdot\vec{\ell}_1+\vec{q}_2\cdot\vec{\ell}_2+\vec{q}_3\cdot\vec{\ell}_3)} \right.$$

$$\left. \varepsilon_{\alpha_1}(1)\varepsilon_{\alpha_2}(2)\varepsilon_{\alpha_3}(3) \right] \times \left[\sum_{\substack{p_1p_2p_3 \\ \beta_1\beta_2\beta_3}} \phi_{\beta_1\beta_2\beta_3}(p_1p_2p_3) e^{i(\vec{q}_1\cdot\vec{p}_1+\vec{q}_2\cdot\vec{p}_2+\vec{q}_3\cdot\vec{p}_3} \right.$$

$$\left. \varepsilon_{\beta_1}(1)\varepsilon_{\beta_2}(2)\varepsilon_{\beta_3}(3) \right] \tag{A9}$$

where $\ell_1 = \vec{R}_{\ell_1}$. Then

$$\bar{\Delta}(\omega_E) = -\frac{1}{6M\hbar^2}[2n(\omega_E)+1]\frac{4}{3\omega_E}\sum_{\substack{q_1q_2q_3\\ \lambda_1\lambda_2\lambda_3}} |V(1,2,3)|^2\,\Delta(q_1+q_2+q_3) \qquad (A10)$$

and since the only dependence on λ is in the polarization vectors we may sum over the λ directly using the orthogonality relations (for Bravais lattices),

$$\sum_{\lambda} \varepsilon_\alpha(q\lambda)\varepsilon_\beta(q\lambda) = \delta_{\alpha\beta}$$

Similarly, only the exponentials in $|V(1,2,3)|^2$ depend upon the wave vectors q_1 and we may sum over these with the result,

$$\sum_{q_1q_2q_3} e^{i\vec{q}_1\cdot(\vec{p}_1-\vec{\ell}_1)}\, e^{i\vec{q}_2\cdot(\vec{p}_2-\vec{\ell}_2)}\, e^{i\vec{q}_3\cdot(\vec{p}_3-\vec{\ell}_3)}\,\Delta(\vec{q}_1+\vec{q}_2+\vec{q}_3)$$

$$= N^2\,\Delta(\ell_3-\ell_1+p_1-p_3)\,\Delta(\ell_3-\ell_2+p_2-p_3)$$

Then

$$\bar{\Delta}(\omega_E) = -\frac{}{36M^3N^2\omega_E^4}[2n(\omega_E)+1]$$

$$\times \sum_{\substack{\ell_1\ell_2\ell_3\\ \alpha_1\alpha_2\alpha_3}} \sum_{p_1} \phi_{\alpha_1\alpha_2\alpha_3}(\ell_1\ell_2\ell_3)\,\phi_{\alpha_1\alpha_2\alpha_3}(p_1, p_1+\ell_2-\ell_1, p_1+\ell_3-\ell_1)\cdot$$

For a two-body potential we must have two of ℓ_1, ℓ_2 or ℓ_3 equal for $\phi(\ell_1\ell_2\ell_3)$ to be non-zero. Using this restriction and translational invariance

$$\bar{\Delta}(\omega_E) = -\frac{\hbar}{12M^3\omega_E^4}\,[2n(\omega_E)+1]\sum_{\ell}\sum_{\alpha\beta\gamma}\phi_{\alpha\beta\gamma}(00\ell)\phi_{\alpha\beta\gamma}(00\ell)\ . \qquad \text{(A11)}$$

The $\phi_{\alpha\beta\gamma}(00\ell)$ is the usual cubic coefficient[1] averaged over the Einstein vibrational distribution. Since the Einstein distribution is spherically symmetric, the averaging does not introduce any additional directional dependence to $\phi_{\alpha\beta\gamma}(00\ell)$ above that already contained in the usual static lattice coefficient.[1] $\phi_{\alpha\beta\gamma}(00\ell)$ therefore has the usual static lattice form with the derivatives averaged. Retaining only the leading, third derivative term.

$$\phi_{\alpha\beta\gamma}(00\ell) \approx \frac{R_\alpha(\ell)R_\beta(\ell)R_\gamma(\ell)}{R^3(\ell)} < \frac{d^3}{dr^3}\, v(R_\ell+u) >_E \qquad \text{(A12)}$$

where $<\ >_E$ is defined in (2.7). Using (A12) the sums over $\alpha\beta\gamma$ in (A11) may then be performed giving,

$$\bar{\Delta}(\omega_E) = -\frac{\hbar}{12M^3\omega_E^4}\,[2n(\omega_E)+1]\sum_{\ell} < \frac{d^3}{dr^3}\, v(R_\ell+u) >_E^2 \qquad \text{(A13)}$$

We expect $\bar{\Delta}(\omega_E)$ to have approximately the same (correct) dependence on mass, temperature and potential as the full expression $\Delta(q\lambda,\omega)$. However, we expect $\bar{\Delta}(\omega_E)$ to be too small in magnitude since $\Delta\alpha\omega^{-4}$. In the full $\Delta(q\lambda,\omega)$ there are many small transverse frequencies which will make $\Delta(q\lambda,\omega)$ large. These small frequencies have all been replaced by a larger ω_E in $\bar{\Delta}(\omega_E)$. To correct for this we multiplied $\bar{\Delta}(\omega_E)$ by a constant so that the iterated SCEC frequency given by (A6) became unstable at the same temperature in Ar as did frequencies given by (A1) for the full SCH + C model. This required multiplying $\bar{\Delta}(\omega_E)$ in (A13) by 2.36.

REFERENCE

(1) R.A. Cowley. Rep. Prog. Phys. 31, 123 (1968).